

# The nucleon mass and pion-nucleon sigma term from a chiral analysis of lattice QCD world data

L. Alvarez-Ruso,<sup>1,\*</sup> T. Ledwig,<sup>2,†</sup> J. Martin Camalich,<sup>3,‡</sup> and M. J. Vicente-Vacas<sup>2,§</sup>

<sup>1</sup>*Instituto de Física Corpuscular (IFIC), Centro Mixto Universidad de Valencia-CSIC, E-46071 Valencia, Spain*

<sup>2</sup>*Departamento de Física Teórica and IFIC, Centro Mixto Universidad de Valencia-CSIC, E-46071 Valencia, Spain*

<sup>3</sup>*Department of Physics and Astronomy, University of Sussex, BN1 9QH, Brighton, UK*

The pion-mass dependence of the nucleon mass within the covariant  $SU(2)$  baryon chiral perturbation theory both without and with explicit  $\Delta(1232)$  degrees of freedom up to order  $p^4$  is investigated. By fitting to lattice QCD data in 2 and 2+1 flavors from several collaborations, for pion masses  $M_\pi < 420$  MeV, we obtain low energy constants of natural size and compatible with pion nucleon scattering data. Our results are consistent with the rather linear pion-mass dependence showed by lattice QCD. In the 2 flavor case we have also performed simultaneous fits to the nucleon mass and  $\sigma_{\pi N}$  data. As a result of our analysis, which encompasses the study of finite volume corrections and discretization effects, we report a value of  $\sigma_{\pi N} = 41(3)(1)$  MeV in the 2 flavor case and  $\sigma_{\pi N} = 52(3)(8)$  MeV for 2+1 flavors, where the inclusion of the  $\Delta(1232)$  resonance changes the results by around 9 MeV. In the 2 flavor case we are able to set independently the scale for lQCD data, given by a Sommer scale of  $r_0 = 0.493(23)$  fm.

PACS numbers: 12.38.Gc, 12.39.Fe, 14.20.Dh

## I. INTRODUCTION

The nucleon mass  $M_N$  is one of the fundamental observables in nature. It arises from the complex and not well understood quark-gluon dynamics in the non-perturbative regime of quantum chromodynamics (QCD). Nevertheless, important progress arises from the interplay of Chiral Perturbation Theory ( $\chi$ PT), the effective theory of QCD at low energies [1–4] and lattice QCD (lQCD) [5], in spite of the technical difficulties to perform lQCD simulation for light-quark masses close to the physical values. This strategy allows to extract some of the parameters of  $\chi$ PT that may not be easily accessible in experiments, clarify the role of baryon resonances in the nucleon selfenergy and unravel its strangeness content [6, 7].

A measure of the contribution from explicit chiral symmetry breaking to the nucleon mass is provided by the so-called sigma terms. In particular, the pion-nucleon  $\sigma_{\pi N}$ -term is defined as

$$\sigma_{\pi N} = \bar{m} \langle N | \bar{u}u + \bar{d}d | N \rangle , \quad (1)$$

in the isospin limit  $m_u = m_d = \bar{m} \approx 4$  MeV. Using the Hellmann-Feynman (HF) theorem,  $\sigma_{\pi N}$  can be related to  $M_N$  [8–10]

$$\sigma_{\pi N} = \bar{m} \frac{\partial}{\partial \bar{m}} M_N(\bar{m}) . \quad (2)$$

Additionally,  $\sigma_{\pi N}$  is the nucleon scalar form factor coming from light quarks at zero four-momentum transfer squared. As such, it enters quadratically in the scattering cross section of supersymmetric dark-matter particles with nucleons. Uncertainties in the determination of sigma-terms, including  $\sigma_{\pi N}$ , currently represent the largest source of error in direct dark-matter searches [11–13].

Traditionally, the pion-nucleon sigma term has been isolated by extrapolating  $\pi N$ -scattering data to the (unphysical) Cheng-Dashen point ( $t = 2M_\pi^2$ ,  $s = u = M_N^2$ , where  $s$ ,  $t$  and  $u$  are the standard Mandelstam variables) [14] using dispersive techniques. The results over the past three decades,  $\sigma_{\pi N} = 49 \pm 8$  MeV [15],  $\simeq 45$  MeV [16],  $56 \pm 9$  MeV [17],  $64 \pm 7$  MeV [18],  $66 \pm 6$  MeV [19],  $43 \pm 12$  MeV [20],<sup>1</sup> depend on the data used as input and on the extrapolation

\*Electronic address: alvarez@ific.uv.es

†Electronic address: ledwig@ific.uv.es

‡Electronic address: j.camalich@sussex.ac.uk

§Electronic address: vicente@ific.uv.es

<sup>1</sup> In the case of Refs. [15, 17–19], to the published value of the sigma-term at the Cheng-Dashen point  $\sigma_{\pi N}(t = 2M_\pi^2)$  we have subtracted  $\Delta_\sigma = \sigma_{\pi N}(t = 2M_\pi^2) - \sigma_{\pi N} = 15.2 \pm 0.4$  according to the dispersive analysis of Ref. [21].

procedure. The lack of consistency among the data sets as well as discrepancies between the parametrizations of the experimental data are a sizable source of systematic uncertainties.

In order to sort the systematic effects out, much effort has been made in the context of baryon  $\chi$ PT (B $\chi$ PT). At a given order in the chiral expansion, B $\chi$ PT allows to express both the nucleon mass (and  $\sigma_{\pi N}$ ) and the  $\pi N$ -scattering amplitude in terms of the same unknown low-energy constants (LECs). The available experimental information on  $\pi N$ -scattering can be used to obtain these LECs. Such a program has encountered a number of difficulties. Unlike in the meson sector, in B $\chi$ PT the power counting (PC) is violated by the presence of  $M_N$  as a heavy scale that does not vanish in the chiral limit. As a consequence, the loop diagrams do not fulfill the naive chiral order dictated by their topology [3]. The solution to this problem follows from noticing that the genuine non-analytic chiral corrections indeed verify the PC, while the breaking pieces are analytic and can be renormalized into the LECs. Different schemes have been developed, including non-relativistic heavy-baryon (HB) [6], and the fully covariant infrared (IR) [22] and extended-on-mass-shell (EOMS) [23, 24]. In HB $\chi$ PT, it was found that the convergence problems in some kinematic regions render the fits insensitive to the leading-order contribution to  $\sigma_{\pi N}$ . The poor convergence can be traced back to the fact that HB limit modifies the analytic structure of the  $\pi N$  amplitude [25]. To overcome the problems of HB $\chi$ PT, the covariant formulations were developed. In the IR approach, loop functions are split into an infrared singular part which fulfills the PC and a regular part, containing the PC-breaking terms and higher order ones, which is dropped. An important drawback is that the IR scheme introduces unphysical cuts [22] which can have disruptive effects in low-energy phenomenology [26, 27]. After applying this method to  $\mathcal{O}(p^4)$ , Becher and Leutwyler concluded that the IR chiral representation of the  $\pi N$ -scattering amplitude is a good approximation only in the subthreshold region so that no reliable determination of the sigma term could be performed from data in the physical region [28]. In the EOMS, the PC is restored by renormalizing the finite number of PC-breaking terms. In this way, the analytic structure of the theory is preserved. Two recent EOMS studies of  $\pi N$  scattering at order  $p^3$  [29] and  $p^4$  [30] have achieved a good description of the data and improved convergence.

A different complication concerns the treatment of the  $\Delta(1232)$   $3/2^+$  resonance which is only  $\sim 300$  MeV heavier than the nucleon and couples strongly to the  $\pi N$  system. In B $\chi$ PT, the  $\Delta(1232)$  is often treated as a heavy state whose influence in the observables is encoded in some of the LECs but, aiming at a more realistic description, it has often been taken explicitly into account. In order to include the  $\Delta(1232)$  as a degree of freedom one needs to define a suitable PC for the new scale  $\Delta = M_\Delta - M_N$  [31–33], and to treat the so-called consistency problem afflicting interacting spin-3/2 fields (see Refs. [34–36] and references therein). The importance of explicitly including the  $\Delta(1232)$  in B $\chi$ PT has been stressed by a recent analysis of the  $\pi N$  scattering amplitude performed in the EOMS scheme [29, 30, 37]. It was shown that the inclusion of the  $\Delta$  resonance in a covariant framework is essential for a reliable extrapolation to the Cheng-Dashen point [37]. The resulting values of  $\sigma_{\pi N}$  are in the 40–60 MeV interval, depending on the partial-wave analysis used as input and in agreement with those obtained by dispersive techniques [29]. Although a value of  $\sigma_{\pi N} = 59 \pm 7$  MeV [29] becomes eventually favored on the grounds of consistency with  $\pi N$  phenomenology [37], an important conclusion of these works is that further efforts are required to understand the possible systematic errors in the  $\pi N$  scattering data.

Another way towards the determination of the  $\pi N$  sigma term is provided by IQCD studies. Two different procedures have been used. In the first one, the matrix element in Eq. (1) is directly obtained and extrapolated to the physical values of the quark masses. The second procedure consists of using Eq. (2), after a suitable extrapolation of IQCD results for  $M_N$  down to the chiral limit. The latter has been favored because of the technical difficulties that arise in the direct determination of disconnected contributions to  $\sigma_{\pi N}$ .

The last decade has witnessed an impressive development of IQCD simulations. Results with two fully dynamical light (as light as possible) degenerate fermions ( $N_f = 2$ ) or with two degenerated light and one heavy (close to the physical strange-quark mass) heavy flavor ( $N_f = 2 + 1$ ) have become standard. Even a direct determination of  $\sigma_{\pi N}$  for  $N_f = 2 + 1 + 1$  (including dynamical  $c$ -quarks) has been reported [38]. Baryon  $\chi$ PT provides a natural framework to extrapolate lattice data for  $M_N$  with heavy quarks down to the physical and chiral limits, provided that the quark masses are small enough to warrant its applicability. In the context of HB $\chi$ PT with a cut-off regularization it was already realized that non-analytic terms were important [39–41]. The quark-mass dependence of  $M_N$  has also been investigated with  $SU(2)$  IR $\chi$ PT to  $\mathcal{O}(p^4)$  without explicit  $\Delta$  [42] and using phenomenological information to constrain the input parameters. Baryon  $\chi$ PT also allows to take finite lattice-volume corrections into account, as it was done for  $M_N$  in Ref. [43]. A more complete  $\mathcal{O}(p^4)$  IR $\chi$ PT study [44] included the leading  $\mathcal{O}(p^3)$  contribution of the  $\Delta$  resonance with the small-scale expansion and HB approximation. According to this work, the introduction of  $\Delta(1232)$  as a propagating degree of freedom is not crucial for  $M_N$ . This is in contrast with the findings of Ref. [45] made with the EOMS scheme up to  $\mathcal{O}(p^3)$ .

More recently, the  $M_\pi$  dependence of new  $N_f = 2$  IQCD data for  $M_N$  has been investigated with HB $\chi$ PT [46] and IR $\chi$ PT without explicit  $\Delta$  degrees of freedom [47–49]. The results for  $\sigma_{\pi N}$  range from 37 to 67 MeV. In the case of Ref. [48], a direct measurement of  $\sigma_{\pi N}$  [50] was incorporated to the fit, which allowed to increase the precision. Furthermore, three new direct determinations of  $\sigma_{\pi N}$  have also been performed applying noise reduction techniques

for a better determination of the disconnected contribution [51].

Several collaborations have pursued IQCD simulations of the masses and  $\sigma_{\pi N}$  using  $N_f = 2+1$  configurations [52–62]. The extrapolation to the physical point allows to determine  $\sigma_{\pi N}$  together with other sigma terms and strangeness content of baryons. The difficulties encountered in HB $\chi$ PT [57, 63] to accomplish this program were overcome applying cut-off regularization schemes [64, 65], using covariant formalisms up to  $\mathcal{O}(p^3)$  [66–68] and  $\mathcal{O}(p^4)$  [69–73], or complementing HB $\chi$ PT with an expansion in the inverse number of colors (large- $N_C$ ) [72, 74, 75]. Although  $SU(3)$ -flavor calculations have reached a considerable degree of maturity, the large number of unknown LECs at  $\mathcal{O}(p^4)$  and the size of the current IQCD data set limits, at present, the accuracy attainable in the sigma terms.

Alternatively,  $SU(2)$  B $\chi$ PT can be used to perform extrapolations of  $M_N$  and  $\sigma_{\pi N}$  in the light-quark masses with the implicit assumption that the influence of the strange quark is embedded in the LECs and that its mass in the simulations is close enough to the physical one. The chiral expansion is expected to converge faster than in  $SU(3)$  B $\chi$ PT and the different LECs appearing at  $\mathcal{O}(p^4)$  can be independently determined using  $\pi N$  scattering. On the other hand, in comparison with the  $N_f = 2$  simulations in which the strange quark is quenched, the extrapolated quantities from  $N_f = 2 + 1$  should be closer to those in the physical world. Analyses of  $N_f = 2 + 1$  simulations with  $SU(2)$ -HB $\chi$ PT ansatzes at  $\mathcal{O}(p^3)$  and without  $\Delta(1232)$  have become standard [63, 76, 77]. In particular, with HB $\chi$ PT up to  $\mathcal{O}(p^4)$  it was found that  $\sigma_{\pi N} = 84 \pm 17 \pm 20$  MeV with explicit inclusion of the  $\Delta$  resonance, and  $\sigma_{\pi N} = 42 \pm 14 \pm 9$  MeV without it [76]. While the inclusion of the  $\Delta$  had little impact on the value of nucleon mass in the chiral limit, the central value of the sigma term changed by a factor of 2. It was also pointed out that the lattice data exhibited a surprisingly linear dependence on  $M_\pi$ , a feature also shown by other IQCD data [57]. The importance of the  $\Delta(1232)$  in extrapolations of IQCD data on  $M_N$  has also been recently stressed in an analysis combining B $\chi$ PT and the large- $N_c$  expansion. [78]. Finally, a different strategy was adopted in Ref. [30], according to which the LECs in  $SU(2)$  B $\chi$ PT up to  $\mathcal{O}(p^4)$  were determined in simultaneous fits to  $\pi N$  scattering data and IQCD results.

Here we present our study of the pion mass dependence of the nucleon mass in covariant  $SU(2)$  B $\chi$ PT up to  $\mathcal{O}(p^4)$ , using the EOMS scheme with explicit inclusion of  $\Delta(1232)$  intermediate states. We perform global fits to recent determinations of  $M_N$  in IQCD simulations with  $N_f = 2$  and  $N_f = 2 + 1$  dynamical quarks, taking into account finite lattice-volume corrections. By extrapolating the fits we determine the nucleon mass in the chiral limit and the pion-nucleon sigma term, paying attention to the different sources of systematic errors: the extrapolation to the continuum of IQCD data with finite lattice spacing, normalization errors, the uncertainties in the LECs fixed in the fits and the range of applicability of the chiral expansion. The article is organized as follows. In Sec. II we describe the formalism, derive the formula for the nucleon mass and discuss the origin of the different coupling constants and LECs that are constrained in the fits. Finite volume corrections and continuum extrapolations are also discussed. The fit strategies and the results are presented in Sec. III. We conclude and summarize our work in Sec. IV. Further details about the calculation can be found in the Appendices.

## II. NUCLEON MASS IN THE B $\chi$ PT

Our aim is to study the pion mass ( $M_\pi$ ) dependence of the nucleon mass ( $M_N$ ) and obtain the value of the  $\sigma_{\pi N}$ -term by means of the HF theorem. For this we employ the  $\mathcal{O}(p^4)$  covariant  $SU(2)$  B $\chi$ PT with and without explicit  $\Delta$ -isobar degrees of freedom,  $\Delta$ B $\chi$ PT and  $\bar{\Delta}$ B $\chi$ PT. The resulting function  $M_N(M_\pi)$  depends on several LECs whose values we fix by fitting IQCD nucleon mass data for unphysical quark-masses. The required ingredients are established in this Section. We derive the perturbative nucleon mass and show the explicit fit formulas together with a discussion of IQCD discretization effects.

To define the nucleon mass in terms of an expansion in the light scales  $m_\pi^2 \equiv 2B\bar{m}$ ,  $p$  and  $\Delta \equiv M_\Delta - M_N$ , we have to choose a counting scheme<sup>2</sup>. If  $\Delta$ -isobars appear explicitly, the common assumptions are the small-scale expansion [31, 32] that counts  $\Delta \sim p \sim m_\pi$  and the  $\delta$ -counting [33], which takes  $\Delta \sim p^{1/2}$  to preserve the hierarchy  $p \sim m_\pi \ll \Delta$ . As the latter is not the case for most of the IQCD simulations, we adopt the small-scale counting. The order  $n$  of a self-energy contribution is then defined by

$$n = 4L - 2N_\pi - N_N - N_\Delta + \sum_k kV_k \quad , \quad (3)$$

for a graph with  $L$  loops,  $N_\pi$  internal pions,  $N_N$  internal nucleons,  $N_\Delta$  internal  $\Delta$ -isobars and  $V_k$  vertices from a  $\mathcal{L}^{(k)}$  Lagrangian. In Fig. 1 we collect all one-particle irreducible diagrams that fulfill, after a suitable renormalization, Eq.

---

<sup>2</sup> The constant  $B$  is proportional to the chiral quark condensate.

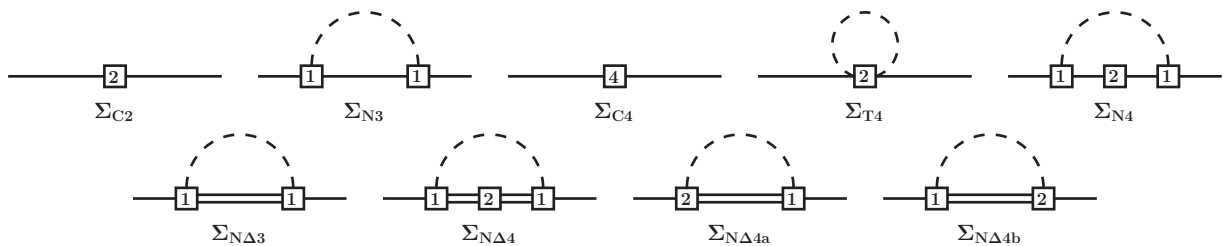


Figure 1: One-particle irreducible contributions to the nucleon self-energy up to  $\mathcal{O}(p^4)$ . Single solid lines denote nucleons, double solid lines,  $\Delta$ -isobars and dashed lines, pions. Boxes represent the pion-nucleon and contact vertices where the number specifies the chiral order.

(3) up to  $n = 4$  [ $\mathcal{O}(p^4)$ ] and list in App. A all relevant B $\chi$ PT Lagrangians. Among the  $\Delta$ -isobar contributions, the graphs  $\Sigma_{N\Delta 4a}$  and  $\Sigma_{N\Delta 4b}$  originate from the  $\mathcal{L}_{\pi N\Delta}^{(2)}$  Lagrangian [29]. It was shown in Ref. [79] for the HB $\chi$ PT case that these couplings are redundant and can be absorbed in the LECs of  $\mathcal{L}_{\pi N}^{(2)}$  and  $\mathcal{L}_{\pi N\Delta}^{(1)}$ . The HB $\chi$ PT expressions are the leading order contributions to covariant B $\chi$ PT results which implies that these two diagrams start to contribute at  $\mathcal{O}(p^5)$ . We do not include them in our  $\mathcal{O}(p^4)$  calculation. Additionally, the  $\pi N$  scattering analysis [29] performed explicit fits with and without these terms and found strong arguments to support that these redundancies also carry over to the covariant case.

To calculate the remaining diagrams we apply the EOMS renormalization-scheme [23, 24] which uses the analyticity of the power-counting breaking terms to overcome the power-counting problem found in [3]. Explicitly, we calculate these diagrams in the dimensional regularization for  $D = 4 - 2\epsilon$  dimensions and renormalize terms proportional to  $L = -\frac{1}{\epsilon} - 1 + \gamma_E - \ln 4\pi$  ( $\overline{MS}$ -scheme). Subsequently, we renormalize the appearing LECs in such a way that power-counting breaking terms are canceled.

### A. Nucleon self-energy and the perturbative nucleon mass

The nucleon physical mass  $M_N$  is defined by the pole position at  $\not{p} = M_N$  of its full propagator

$$\frac{1}{\not{p} - M_0 - \Sigma(\not{p})} \quad , \quad (4)$$

where  $\Sigma(\not{p})$  and  $M_0$  are the nucleon self-energy and the (chiral limit) bare mass. In order to define a perturbative nucleon mass, we expand  $\Sigma(\not{p})$  around  $\not{p} = M_0$ :

$$\Sigma(\not{p}) = \Sigma(M_0) + (\not{p} - M_0) \left. \frac{\partial}{\partial \not{p}} \right|_{\not{p}=M_0} \Sigma(\not{p}) + \frac{1}{2} (\not{p} - M_0)^2 \left. \frac{\partial^2}{\partial \not{p}^2} \right|_{\not{p}=M_0} \Sigma(\not{p}) + \dots \quad (5)$$

$$= \Sigma(M_0) + (\not{p} - M_0) \Sigma'(M_0) + R(\not{p}) \quad , \quad (6)$$

and write the propagator as

$$\frac{1}{\not{p} - M_0 - \Sigma(\not{p})} = \frac{1}{\not{p} - M_0 - \frac{\Sigma(M_0)}{1 - \Sigma'(M_0)} - \frac{R(\not{p})}{1 - \Sigma'(M_0)}} \frac{1}{1 - \Sigma'(M_0)} \quad . \quad (7)$$

Equation (7) defines now the nucleon mass by the pole at  $\not{p} = M_N$

$$M_N = M_0 + Z \Sigma(M_0) + Z R(M_N) \quad , \quad (8)$$

together with its residue

$$Z = \frac{1}{1 - \Sigma'(M_0)} \quad . \quad (9)$$

Using the B $\chi$ PT self-energies up to order  $p^4$  of App. B gives:

$$\Sigma_{p^4}(\not{p}) = \Sigma^{(2)} + \Sigma^{(3)}(\not{p}) + \Sigma^{(4)}(\not{p}) \quad (10)$$

$$= \Sigma^{(2)} + \Sigma^{(3)}(M_0) + \Sigma^{(4)}(M_0) + (\not{p} - M_0) \left[ \Sigma^{(3)'}(M_0) + \Sigma^{(4)'}(M_0) \right] + R(\not{p}) \quad , \quad (11)$$

$$Z = 1 + \Sigma^{(3)'}(M_0) + \mathcal{O}(p^3) \quad , \quad (12)$$

where the upper indices denote the chiral order. Only the contact term  $\Sigma_{C2} = -4c_1 m_\pi^2$  enters in  $\Sigma^{(2)}$  so it does not depend on  $\not{p}$ . Inserting Eq. (11) in Eq. (8) one gets the nucleon mass up to order  $p^4$ :

$$\begin{aligned} M_N^{(4)}(m_\pi^2) &= M_0 + \Sigma_{C2}(m_\pi^2) + \Sigma_{N3}(m_\pi^2) + \Sigma_{N\Delta3}(m_\pi^2) \\ &\quad + \Sigma_{N4}(m_\pi^2) + \Sigma_{T4}(m_\pi^2) + \Sigma_{C4}(m_\pi^2) + \Sigma_{C2}(m_\pi^2) \Sigma'_{N3}(m_\pi^2) \\ &\quad + \Sigma_{N\Delta4}(m_\pi^2) + \Sigma_{C2}(m_\pi^2) \Sigma'_{N\Delta3}(m_\pi^2) + \mathcal{O}(p^5) \ , \end{aligned} \quad (13)$$

where all loops are evaluated at  $\not{p} = M_0$ . The term  $R(M_N)$  contributes only at  $\mathcal{O}(p^5)$ . The first line of Eq. (13) corresponds to the  $p^3$  nucleon mass while the second and third lines are the additional  $p^4$  contributions; the notation of the different terms matches the one of the diagrams in Fig. 1. All  $\Sigma_i$  are obtained from the Lagrangians in App. A and are explicitly given in App. B. There are 10 low energy constants, namely,  $f_{\pi 0}, g_{A0}, c_1, c_2, c_3, h_{A0}, M_0, M_{\Delta 0}, c_{1\Delta}, \alpha$ . Most of them are constrained by experimental data. More details about their treatment are given below.

## B. Nucleon mass, $\sigma_{\pi N}$ -term and fit formula

Applying the HF theorem

$$\sigma_{\pi N}(m_\pi^2) = \bar{m} \frac{\partial}{\partial \bar{m}} M_N(\bar{m}) = m_\pi^2 \frac{\partial}{\partial m_\pi^2} M_N(m_\pi^2) \quad (14)$$

to Eq. (13) one obtains,

$$M_N^{(4)}(m_\pi^2) = M_0 - c_1 4m_\pi^2 + \frac{1}{2} \alpha m_\pi^4 + \Sigma_{loops}^{(3)+(4)}(m_\pi^2, M_0, M_{\Delta 0}, f_{\pi 0}, g_{A0}, h_{A0}, c_i) \ , \quad (15)$$

$$\sigma_{\pi N}^{(4)}(m_\pi^2) = -4c_1 m_\pi^2 + \alpha m_\pi^4 + m_\pi^2 \frac{\partial}{\partial m_\pi^2} \Sigma_{loops}^{(3)+(4)}(m_\pi^2, M_0, M_{\Delta 0}, f_{\pi 0}, g_{A0}, h_{A0}, c_i) \ , \quad (16)$$

with  $c_i = c_1, c_2, c_3, c_{1\Delta}$ . The  $\sigma_{\pi N}^{(4)}$  can also be obtained from a direct calculation of the nucleon scalar form factor Eq. (1) at zero four-momentum transfer squared. We have checked that Eq. (16) can be mapped term by term to such a calculation, i.e. that our formulas with full, non-expanded loops fulfill the HF theorem.

To apply Eqs. (15,16) with a  $p^4$  accuracy, we cannot identify the physical (or lattice) pion mass  $M_\pi$  with the lowest order  $m_\pi$  ( $M_\pi^2 = m_\pi^2 = 2B\bar{m}$ ) but must take the next order into account. According to the well known expansion [2]:

$$M_\pi^2(m_\pi^2) = m_\pi^2 + \frac{2l_3^r(\Lambda^2)}{f_{\pi 0}^2} m_\pi^4 + \frac{1}{32\pi^2 f_{\pi 0}^2} m_\pi^4 \ln \frac{m_\pi^2}{\Lambda^2} + \mathcal{O}(p^6) \ , \quad (17)$$

where  $l_3^r(\Lambda^2)$  is a renormalized scale-dependent LEC coming from the meson  $\chi$ PT Lagrangian. Therefore

$$M_N^{(4)}(M_\pi^2) = M_0 - c_1 4M_\pi^2 + \frac{1}{2} \bar{\alpha} M_\pi^4 + \frac{c_1}{8\pi^2 f_\pi^2} M_\pi^4 \ln \frac{M_\pi^2}{M_0^2} + \Sigma_{loops}^{(3)+(4)}(M_\pi^2, M_0, M_{\Delta 0}, f_\pi, g_A, h_A, c_i) + \mathcal{O}(p^5) \ , \quad (18)$$

$$\begin{aligned} \sigma_{\pi N}^{(4)}(M_\pi^2) &= -4c_1 M_\pi^2 + \bar{\alpha} M_\pi^4 - c_1 \frac{8}{f_\pi^2} l_3^r(M_0^2) M_\pi^4 + \frac{c_1}{8\pi^2 f_\pi^2} M_\pi^4 \ln \frac{M_\pi^2}{M_0^2} \\ &\quad + M_\pi^2 \frac{\partial}{\partial M_\pi^2} \Sigma_{loops}^{(3)+(4)}(M_\pi^2, M_0, M_{\Delta 0}, f_\pi, g_A, h_A, c_i) + \mathcal{O}(p^5) \end{aligned} \quad (19)$$

$$\text{with} \quad \bar{\alpha} = \alpha + c_1 \frac{16}{f_\pi^2} l_3^r(M_0^2) \ . \quad (20)$$

Equation (18) is our final formula for  $\mathcal{O}(p^4)$  B $\chi$ PT fits to lQCD data. The effect of Eq. (17) is an additional  $\mathcal{O}(p^4)$  term proportional to  $c_1$  and a redefinition of  $\alpha \rightarrow \bar{\alpha}$  which will be a fit parameter. Furthermore, we adopt the physical values of  $f_\pi = 92.4$  MeV and  $g_A = 1.267$  instead of the chiral limit ones and set the renormalization scale to  $\Lambda = M_0$ . The differences between the chiral limit and physical values are of order  $p^2$  so that they start to contribute at  $\mathcal{O}(p^5)$ . In the case of  $\sigma_{\pi N}^{(4)}(M_\pi^2)$  we cannot absorb all terms proportional to  $l_3^r(M_0^2)$  in the LECs and shall need a numerical value for it. From the latest estimate of  $\bar{l}_3(M_\pi) = \ln \Lambda_3^2 / M_\pi^2$  at the physical point  $\bar{l}_3(139 \text{ MeV}) = 3.2(8)$  [2, 80] one has:

$$l_3^r(\Lambda^2) = -\frac{1}{64\pi^2} \left( \bar{l}_3(M_\pi) + \ln \frac{M_\pi^2}{\Lambda^2} \right) = -\frac{1}{64\pi^2} \left( 3.2(8) + \ln \frac{M_\pi^2(p_{phys})}{\Lambda^2} \right) \ , \quad (21)$$

where we set  $M_{\pi(p_{phys})} = 139$  MeV.

Theory	$c_2$ [GeV <sup>-3</sup> ]	$c_3$ [GeV <sup>-3</sup> ]	$c_{1\Delta}$ [GeV <sup>-3</sup> ]	$h_A$	$M_{\Delta 0}$ [MeV]
$\bar{\Delta}$ -B $\chi$ PT	$3.9 \pm 0.4$	$-6.7 \pm 0.4$	--	--	--
$\Delta$ -B $\chi$ PT	$1.1^{+0.2}_{-0.5}$	$-3.0^{+0.6}_{-0.1}$	$-0.90 \pm 40$	2.87	$1170 \pm 30$

Table I: Values of the LECs appearing in the  $p^4$  nucleon mass. For the LECs  $f_{\pi 0}$  and  $g_{A0}$  we take their physical values  $f_{\pi} = 92.4$  MeV and  $g_A = 1.267$ .

### C. Low-energy constants, finite volume and lattice spacing effects

After fixing  $f_{\pi 0}$  and  $g_{A0}$ , we discuss our treatment of the remaining eight LECs,  $c_1$ ,  $c_2$ ,  $c_3$ ,  $M_0$ ,  $\bar{\alpha}$ ,  $M_{\Delta 0}$ ,  $h_{A0}$ , and  $c_{1\Delta}$ . Generally, our fits depend very mildly on variations in  $c_2$ ,  $c_3$ ,  $M_{\Delta 0}$  and  $h_A$ . Furthermore, we observe that changes in  $c_{1\Delta}$  are compensated by changes in  $\bar{\alpha}$ . Our strategy is, therefore, to fit  $M_0$ ,  $c_1$  and  $\bar{\alpha}$  while keeping  $c_2$ ,  $c_3$ ,  $M_{\Delta 0}$ ,  $h_A$  and  $c_{1\Delta}$  fixed. The nucleon-related LECs  $c_2$  and  $c_3$  are taken from the  $\pi N$ -scattering analysis of Ref. [37], performed with the same B $\chi$ PT framework employed here. More specifically, we take as central values the average of the results of fits to the phase shifts from the Karlsruhe-Helsinki group (KA85) and the George Washington University group (WI08), accepting errors defined by their uncertainties and also by the result of the fit to Matsinos phase shifts (EM06) (see Tables 1 and 2 of Ref. [37])<sup>3</sup>. The specific figures for both the  $\bar{\Delta}$ -B $\chi$ PT and  $\Delta$ -B $\chi$ PT cases are given in Table I.

In order to fix the  $\Delta$ -related LECs,  $M_{\Delta 0}$ ,  $c_{1\Delta}$  and  $h_A$ , we consider the pion-mass dependence of the  $\Delta$ -isobar mass. Up to  $\mathcal{O}(p^3)$  it reads [45]

$$M_{\Delta}^{(3)}(M_{\pi}) = M_{\Delta 0} - 4c_{1\Delta}M_{\pi}^2 + \Sigma_{\Delta N 3}(M_{\pi}; h_A, f_{\pi}, M_N, M_{\Delta}) + \Sigma_{\Delta \Delta 3}(M_{\pi}; H_A, f_{\pi}, M_{\Delta}) \quad , \quad (22)$$

where the loop contributions  $\Sigma_{\Delta N 3}$  and  $\Sigma_{\Delta \Delta 3}$  stand for diagrams like  $\Sigma_{N 3}$  and  $\Sigma_{N \Delta 3}$  in Fig 1 but with external nucleon lines replaced by  $\Delta(1232)$  ones. The explicit expressions are given in App. B. Since differences are of higher order, we are allowed to take phenomenological values for the LECs in these loops, instead of the leading-order ones. In this way, one uses the phenomenological value of the  $\Delta$ -isobar decay width  $\Gamma_{\Delta \rightarrow N\pi} = -2 \text{Im}\Sigma_{\Delta N 3} = 115$  MeV to fix  $h_A = 2.87$ . Furthermore, we adopt  $H_A = \frac{9}{5}g_A$  obtained in the large- $N_c$  limit. Finally, we use lQCD data for the  $\Delta(1232)$  [52, 53, 81] mass to determine the remaining two LECs  $M_{\Delta 0}$  and  $c_{1\Delta}$ . As the available lattice results are rather scattered, we do not perform a rigorous fit to them but, instead, adopt the conservative attitude of setting a band that englobes all the lQCD points with their errorbars (see Fig. 2). The central values for the parameters result from the average of those defining the band's boundaries and are listed in Table I.

We now turn to two discretization artifacts: finite volume (FV) and finite spacing effects, appearing in lQCD studies, as a consequence of the finite grid with volume  $L^3$  and spacing  $a$  in which simulations are performed.

All loop graphs of Fig. 1 are subject to FV corrections. We calculate them in App. B3 applying the standard techniques of Ref. [43]. The FV corrections to  $\Sigma_{N 3}$  and  $\Sigma_{T 4}$  are equivalent to those in Ref. [43]. In addition, we correct the combination  $\Sigma_{N 4} + \Sigma_{c 2}\Sigma'_{N 3}$ , the  $\Delta$ -isobar graphs  $\Sigma_{N \Delta 3}$ ,  $\Sigma_{N \Delta 4}$  and  $\Sigma_{C 2}\Sigma'_{N \Delta 3}$  which contribute at order  $p^4$  in the continuum [23, 24] in the EOMS renormalization scheme. Reference [43] employs IR, for which the combination of  $\Sigma_{N 4} + \Sigma_{c 2}\Sigma'_{N 3}$  appears only at order  $p^5$ . Our FV corrections are therefore:

$$\begin{aligned} \Sigma_{p^4}(M_{\pi}^2, L) = & \Sigma_{N 3}(M_{\pi}^2, L) + \Sigma_{N \Delta 3}(M_{\pi}^2, L) \\ & + \Sigma_{N 4}(M_{\pi}^2, L) + \Sigma_{N \Delta 4}(M_{\pi}^2, L) + \Sigma_{T 4}(M_{\pi}^2, L) \\ & + \Sigma_{C 2}(M_{\pi}^2) \Sigma'_{N 3}(M_{\pi}^2, L) + \Sigma_{C 2}(M_{\pi}^2) \Sigma'_{N \Delta 3}(M_{\pi}^2, L) \quad . \end{aligned} \quad (23)$$

All these terms are given in App. B3. In Fig. 3 we test our FV correction against lQCD data with approximately the same pion mass but different  $L$ . We found four points from the QCDSF collaboration [48], four points from the NPLQCD collaboration [61] and two points from the ETMC collaboration [82] at pion masses approximately of 265, 300, 390 and 440 MeV, respectively. Reasonable values of the LECs  $M_0 = 890$  MeV and  $c_1 = c_{1\Delta} = -0.9$  GeV<sup>-1</sup> have been chosen for this exercise. We observe that our FV corrections describe very well the  $L$  dependence for lattice sizes larger than  $\sim 2.2$  fm and that they have a size of up to 45 MeV. In our fits we shall include only data points with  $LM_{\pi} > 3.8$  for all of which  $L > 2.2$  fm.

In general, we will use lQCD data that are not extrapolated to the continuum limit  $a \rightarrow 0$ . Originally, discretized QCD actions break chiral symmetry even in the chiral limit by terms proportional to  $a$  [83–85] but modern lattice

<sup>3</sup> Further justification for this choice is given in the Results Section.

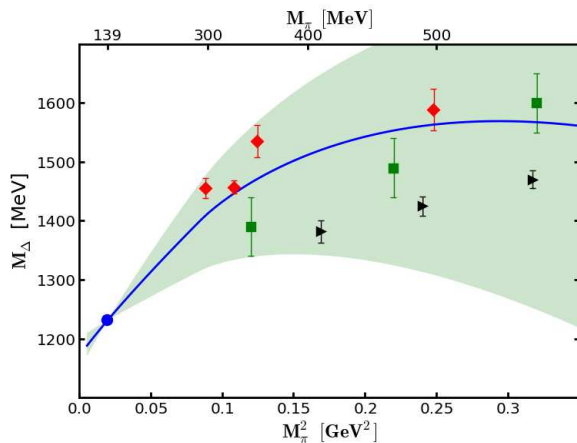


Figure 2: Pion mass dependence of the  $\Delta$ -isobar mass. Green squares are from [52, 53], black right-triangles are quenched data from [81] and red diamonds are unquenched data from [81]. The blue circle is the physical point. The band defines the uncertainty range adopted (see the text) while the blue line is the preferred result.

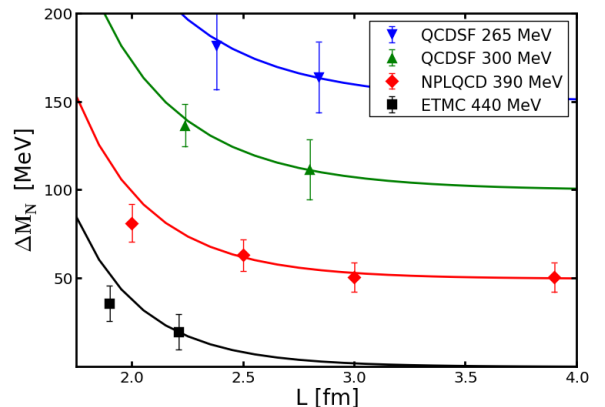


Figure 3: Finite volume corrections  $\Delta M_N = M_N(L) - M_N(L \rightarrow \infty)$  as a function of the lattice size for pion masses of 265 MeV, 300 MeV, 390 MeV and 440 MeV. Lattice data from Refs. [48] (triangles), [61] (red diamonds) and [82] (squares) with approximately the same pion masses are also displayed. We normalized each curve to the point with the largest volume and shifted them by multiples of 50 MeV to avoid overlaps. At  $L = 4.0$  fm  $\Delta M_N \approx 0$  for all curves.

calculations use  $\mathcal{O}(a)$  improved actions for which discretization effects in baryon masses start at order  $a^2$ . However, there exists a whole variety of lQCD-actions, each with its own discretization effects. For the specific Symanzik lQCD action an effective field theory investigation has been performed in Ref. [86] on a HB $\chi$ PT basis but a general approach, similar to the treatment of FV corrections, does not exist. Therefore, we parametrize this effect for each action individually by writing the nucleon mass in an  $a$ -expansion to the lowest order as

$$M_N = M_{a=0} + c_a a^2 + \mathcal{O}(a^3, a^2 m_\pi^2) \quad , \quad (24)$$

with an action-specific constant  $c_a$ . By using the ETMC points at  $M_\pi = 260$  and  $262$  MeV, and QCDSF points at  $r_0 M_\pi = 0.658$  and  $0.660$  [48, 82] we can roughly estimate the size of this effect. By taking the linear  $a^2$ -extrapolation of Eq. (24) we obtain  $c_{ETMC} = 0.17$  GeV<sup>3</sup> and  $c_{QCDSF} = 0.33$  GeV<sup>3</sup>, which correspond to nucleon-mass shifts of 10 – 50 MeV. We obtain that lattice spacing corrections can have similar sizes as the FV ones. Therefore, we incorporate this effect in specific fits by including the  $c_a a^2$  term in the  $\chi^2$  for each collaboration/action reporting results for different values of  $a$ .

### III. RESULTS

We study the pion mass dependence of the nucleon mass by using the covariant B $\chi$ PT expression of Eqs. (13) and (18), which is accurate up to the chiral order  $p^4$  and includes explicit  $\Delta$ -isobar degrees of freedom. We perform global fits to lQCD ensembles for  $N_f = 2$  and  $N_f = 2+1$  numbers of flavors. Generally, lQCD uses a discretized QCD-action to simulate the quark-gluon interaction in a finite box of size  $L^3 \times T$  with finite spatial and time spacings of  $a$  and  $a_t$ . The nucleon mass data are given in terms of the dimensionless quantities  $aM_\pi$  and  $aM_N$  with uncertainties in  $a$ ,  $aM_\pi$  and  $aM_N$ . An actual value of  $a$  sets the overall scale to convert the lQCD data into physical units. No universal scale-setting method exists and different collaborations use different approaches. Furthermore, the statistical uncertainty in  $a$  turns into a normalization uncertainty in  $M_N$  for data points belonging to the same  $a$ -set. It is therefore preferable to fit the  $(aM_\pi, aM_N)$  data directly whenever this is possible or, otherwise, to include these correlated uncertainties in the fit. As explained below, we are able to perform the former in the case of the  $N_f = 2$  ensembles and rely on the latter for the  $N_f = 2+1$  ones. We also include FV corrections and lattice spacing effects as described in the previous section. We fit the LECs  $M_0$ ,  $c_1$  and  $\bar{\alpha}$  while keeping  $c_2$ ,  $c_3$ ,  $c_{1\Delta}$ ,  $h_A$  and  $M_{\Delta 0}$  fixed to the values listed in Tab. I. Afterwards, we quantify the effect of varying the fixed LECs within their ranges. The fit uncertainties are determined at a 68% confidence level.

For  $N_f = 2$  we include data from the BGR [87], ETMC [82], Mainz [88] and QCDSF [48] collaborations, and for  $N_f = 2 + 1$  from the BMW [59], HSC [58], LHPC [56], MILC [89], NPLQCD [61], PACS [90] and RBCUK-QCD [62] collaborations. In both cases we extract the LECs and obtain the  $\sigma_{\pi N}$  value by using the HF theorem.

### A. Nucleon mass up to order $\mathcal{O}(p^4)$ : fits to $N_f = 2$ lattice QCD data

We use Eq. (18) to fit the lQCD data for the  $N_f = 2$  ensembles of the BGR, ETMC, Mainz and QCDSF collaborations [48, 82, 87, 88]. The lQCD data are given in terms of the dimensionless products  $aM_\pi$  and  $aM_N$  where the scale is fixed in different ways: with the experimental  $\Omega^-$  mass in Ref. [88] and with HB $\chi$ PT or IR- $\chi$ PT chiral extrapolations of  $M_N$  in Refs. [48, 82]. The available information for these data sets is such that we can perform our own scale setting. By doing this we compensate for the different scales of the various sets and avoid to manipulate them with two different B $\chi$ PT versions.

Explicitly, we fit the lQCD data in terms of  $(r_0 M_\pi, r_0 M_N)$  by using the Sommer-scale  $r_0$  [91] and the ratios  $r_0/a$  in the chiral limit, as reported by each Collaboration. The uncertainties in  $aM_\pi$ ,  $aM_N$  and  $r_0/a$  are assumed to be uncorrelated. The value of  $r_0$  is a priori unknown and we determine it recursively inside the fit. This is the same strategy used in Ref. [48], now employed to analyze  $N_f = 2$  data globally. The  $\chi^2$  function that we minimize is

$$\chi^2 = \sum_i \left[ \frac{\widetilde{M}_N^{(n)}(\widetilde{M}_\pi^2) + \widetilde{\Sigma}_N^{(n)}(\widetilde{M}_\pi^2, L) + \widetilde{c}_a \widetilde{a}^2 - d_i(\widetilde{M}_\pi^2, L)}{\sigma_i} \right]^2, \quad (25)$$

$$\text{with } \widetilde{M}_N^{(n)} = r_0 M_N^{(n)}, \quad \widetilde{M}_\pi^2 = (r_0 M_\pi)^2, \quad \widetilde{\Sigma}_N^{(n)} = r_0 \Sigma_N^{(n)}, \quad (26)$$

where  $d_i(\widetilde{M}_\pi^2, L)$  are the lQCD data points with uncertainties  $\sigma_i$ , each of them generated in a lattice of size  $L$  and spacing  $a$ . The continuum expressions  $M_N^{(n)}(M_\pi^2)$  and the finite volume corrections  $\Sigma^{(n)}(M_\pi^2, L)$  for the chiral-order  $n$  are listed in App. B 4. As discussed above, the terms  $\widetilde{c}_a \widetilde{a}^2 = r_0^3 c_a (a/r_0)^2$  parametrize discretization effects, with  $c_a$  being common constants for points obtained by the same lQCD Collaboration/action. The Sommer-scale is calculated in each minimization step recursively using the constrain imposed by the experimental value of the nucleon mass at the physical point:

$$r_0^k = \frac{\widetilde{M}_N^{(n)}(r_0^{k-1} \cdot M_{\pi(\text{phys})})}{M_{N(\text{phys})}} \quad \text{until} \quad |r_0^k - r_0^{k-1}| < 0.001 \text{ fm} . \quad (27)$$

The explicit fit parameters in Eq. (25) are  $M_0$ ,  $c_1$ ,  $\bar{a}$  and two  $c_a$  constants, one for the ETMC Collaboration and one for both Mainz and QCDSF which employ the same action. The single data point of BGR does not allow to perform any lattice spacing correction. As the term  $\widetilde{c}_a \widetilde{a}^2$  does not stand on the same firm ground, from the perspective of effective field theory, as the rest of our mass formula, we perform fit with and without it and treat the differences as systematic errors. We restrict the data sets by imposing the following conditions:  $r_0 M_\pi < 1.11$ ,  $M_\pi L > 3.8$ , which englobe points of  $M_\pi < (429, 476)$  MeV for Sommer-scale values in the range  $r_0 = (0.51, 0.46)$  fm. We then consider the following data sets

- BGR [87]: A Sommer-scale of  $r_0 = 0.48$  fm is assumed and three data points are provided, only one below  $r_0 M_N = 1.11$ .
- ETMC [82]: Eleven data points are provided in the form  $(aM_\pi, aM_N)$ ; for each setting a value of  $r_0/a$  is computed. After converting  $(aM_\pi, aM_N)$  into  $(r_0 M_\pi, r_0 M_N)$  we find that seven data points fulfill our conditions and enter the fit.
- Mainz [88]: Eleven data points are provided in the form  $(aM_\pi, aM_N)$ . The lattice spacings as well as the ratios  $r_0/a$  are determined by the  $\Omega^-$  mass [92, 93]. We convert  $(aM_\pi, aM_N)$  to  $(r_0 M_\pi, r_0 M_N)$  and six data points enter the fit.
- QCDSF [48]: This work provides 27 data points, directly in terms of  $(r_0 M_\pi, r_0 M_N)$ , but only two of them fulfill our restrictions. In addition, there is a single data point for the  $\sigma_{\pi N}$  obtained by direct determination at  $M_\pi \sim 285$  MeV [50].

We study the following variations of the fits:

1.  $M_N(M_\pi)$  to order  $p^2$ ,  $p^3$  and  $p^4$  in the chiral expansion



	excluding $\sigma_{\pi N}$ (285 MeV)						including $\sigma_{\pi N}$ (285 MeV)					
	$M_0$ [MeV]	$c_1$ [ $\text{GeV}^{-1}$ ]	$\bar{\alpha}$ [ $\text{GeV}^{-3}$ ]	$\frac{\chi^2}{dof}$	$r_0$ [fm]	$\sigma_\pi$ [MeV]	$M_0$ [MeV]	$c_1$ [ $\text{GeV}^{-1}$ ]	$\bar{\alpha}$ [ $\text{GeV}^{-3}$ ]	$\frac{\chi^2}{dof}$	$r_0$ [fm]	$\sigma_\pi$ [MeV]
$p^2$	906 (11)	-0.43 (2)	-	2.1	0.509	34 (2)	913 (6)	-0.33 (1)	-	6.3	0.539	26 (1)
$p^3$	880 (13)	-0.93 (3)	-	1.9	0.480	53 (2)	892 (6)	-0.78 (1)	-	8.5	0.527	41 (1)
$p^3_\Delta$	863 (16)	-1.19 (4)	-	2.1	0.456	68 (3)	878 (5)	-1.00 (1)	-	9.5	0.517	52 (1)
$p^4$	866 (40)	-1.18 (14)	23 (3)	2.5	0.470	62 (13)	888 (9)	-0.91 (4)	38 (2)	2.9	0.507	41 (3)
$p^4_\Delta$	893 (29)	-0.77 (9)	35 (2)	2.4	0.494	38 (10)	890 (7)	-0.80 (1)	33 (2)	2.5	0.489	41 (2)

Table II: Results for  $B\chi$ PT fits to  $N_f = 2$  nucleon mass data from Refs. [48, 82, 87, 88]. The ' $\Delta$ ' index denotes the inclusion of explicit  $\Delta$ -isobar ( $\Delta B\chi$ PT), while its omission corresponds to  $\Delta B\chi$ PT; FV corrections are included but finite-spacing effects are excluded. The left-panel results come from a fit of solely nucleon-mass data while in the right panel the  $\sigma_{\pi N}$  point at  $M_\pi = 285$  MeV of Ref [50] was also taken into account.

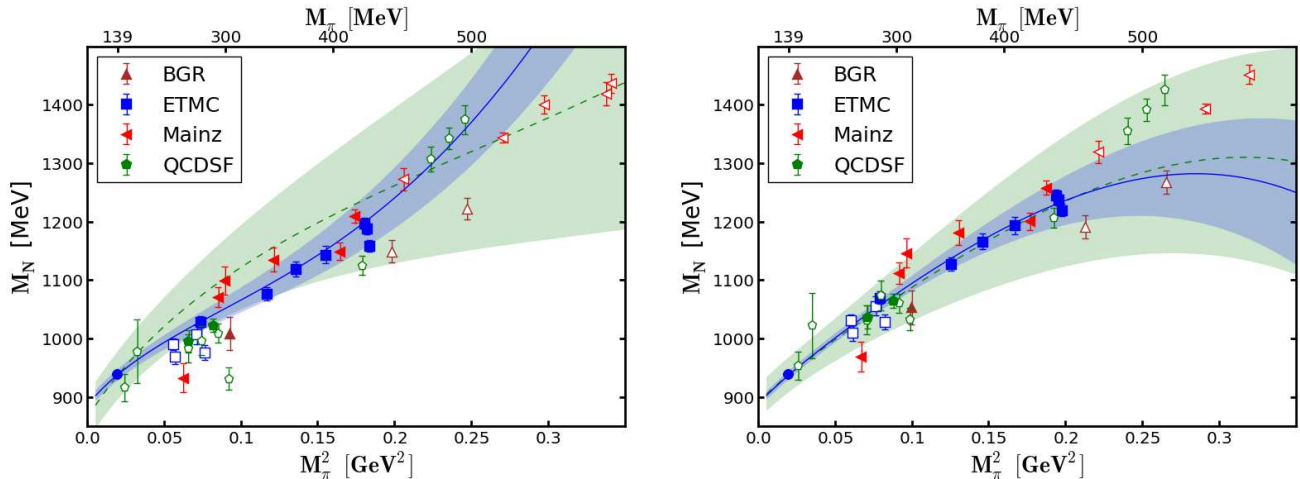


Figure 4: Fits to the  $N_f = 2$  nucleon mass data of Refs. [48, 82, 87, 88]. Filled (open) symbols are for data points included in (excluded from) the fits. The left (right) picture shows fits without (with) explicit  $\Delta$ -isobar. The fit including the  $\sigma_{\pi N}$  (285 MeV) of Ref. [50] is given by the blue solid line while the plain nucleon mass fit is given by the green dashed one. The dark blue and light green shaded regions represent the corresponding statistical uncertainties. The IQCD data are scaled by  $r_0$  and FV corrected according to the simultaneous fit. Hence, the green dashed line does not correspond to the shown data points.

2. without ( $\Delta B\chi$ PT) and with ( $\Delta B\chi$ PT)  $\Delta$ -isobar
3. including and excluding the single direct  $\sigma_{\pi N}$  measurement of Ref. [50]
4. without and with lattice spacing corrections ( $c_a a^2$  term)
5. variations of the input LECs according to the errors quoted in Table I

Finite volume corrections are always included.

The output of our fits for cases 1-3, with the LECs fixed to the values in Table I and without lattice-spacing corrections are presented in Table II and Fig. 4. Bear in mind that changes in the fit conditions 1 and 2 yield different  $r_0$  (see Table II) so IQCD data are scaled differently. From Table II we observe that the inclusion of  $\mathcal{O}(p^4)$  does not lead to a better description of present nucleon mass data than the  $\mathcal{O}(p^3)$  one. However, for fits including the  $\sigma_{\pi N}$  (285) point, a good  $\chi^2/dof$  emerges only at  $\mathcal{O}(p^4)$ . In this situation,  $\Delta B\chi$ PT gives a slightly better  $\chi^2/dof$  than  $\Delta B\chi$ PT but both approaches give the same  $\sigma_{\pi N}$  value. The overall rather high  $\chi^2/dof$  is caused by two points from the Mainz Collaboration. By excluding them we obtain  $\chi^2/dof \sim 1.6$  but the results change only within the quoted uncertainties. The FV corrections shift the data points by  $(-6) - (-50)$  MeV. In contrast to the  $\Delta B\chi$ PT case, the  $\Delta B\chi$ PT  $p^4$ -results are not significantly altered by the inclusion of  $\sigma_{\pi N}$  (285) in the fits and exhibit a softer  $M_\pi$  dependence. This might be interpreted as an indication that the theory with explicit  $\Delta(1232)$  is more realistic.

Figure 5 shows the relative contributions,  $|p^3/p^2|$  and  $|p^4/p^3|$ , of different chiral orders to the nucleon mass for fits including  $\sigma_{\pi N}$  (285). One observes that the  $\mathcal{O}(p^4)$  term has a relatively small contribution over a large  $M_\pi$  range. The same is true for the  $\Delta B\chi$ PT  $\mathcal{O}(p^3)$  term. In the  $\Delta B\chi$ PT case, however, the relative impact of the  $\mathcal{O}(p^3)$  contribution

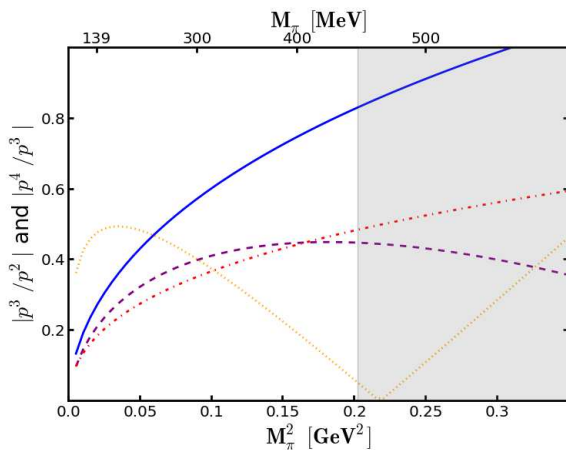


Figure 5: The  $B\chi$ PT results for  $M_N(M_\pi)$  decomposed into their chiral-order relative contributions  $|p^3/p^2|$  and  $|p^4/p^3|$ . The blue solid line denotes  $|p^3/p^2|$  and the purple-dashed line,  $|p^4/p^3|$ , both for  $\Delta B\chi$ PT. The red dashed-dotted and orange dotted are the  $|p^3/p^2|$  and  $|p^4/p^3|$  results for  $\Delta B\chi$ PT. The shaded region is excluded from the fit.

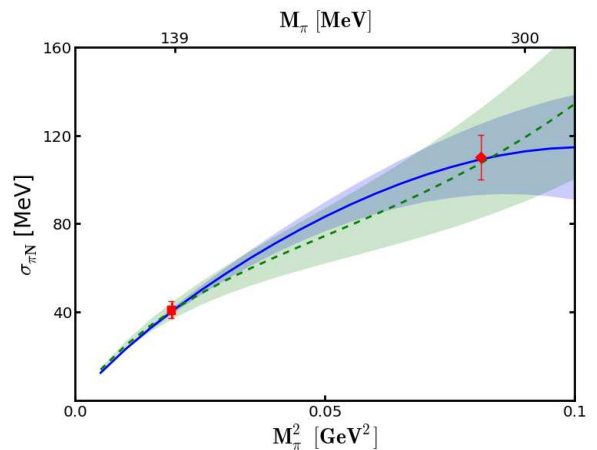


Figure 6: Pion-mass dependence of the  $\sigma_{\pi N}$ -term. The blue solid line and the green dashed lines stand for the  $\Delta B\chi$ PT and  $\Delta B\chi$ PT fits respectively, both including  $\sigma_{\pi N}(285)$  of Ref [50] (red diamond). The dark blue and light green shaded areas represent the corresponding uncertainties. The red square is our final result at the physical point.

$p_\Delta^4$	$M_0$ [MeV]	$c_1$ [ $\text{GeV}^{-1}$ ]	$\bar{\alpha}$ [ $\text{GeV}^{-3}$ ]	$c_E$ [ $\text{GeV}^{-3}$ ]	$c_{MQ}$ [ $\text{GeV}^{-3}$ ]	$\frac{\chi^2}{d.o.f}$	$r_0$ [fm]	$\sigma_\pi$ [MeV]
excluding $\sigma_{\pi N}(285 \text{ MeV})$	894 (28)	-0.76 (10)	36 (5)	-0.06 (7)	-0.05 (13)	2.8	0.501	37 (10)
including $\sigma_{\pi N}(285 \text{ MeV})$	892 (21)	-0.79 (2)	34 (3)	-0.08 (6)	-0.08 (12)	2.8	0.499	40 (3)

Table III: Results for  $p^4$ - $\Delta B\chi$ PT fits to  $N_f = 2$  nucleon mass data from Refs. [48, 82, 88] with lattice spacing effects accounted by the  $c_E a^2$  and  $c_{MQ} a^2$  terms for the ETMC and Mainz/QCDSF data respectively.

steadily rises, becoming more than 80% of the  $p^2$  one at  $M_\pi > 450$  MeV. From this we deduce that  $M_\pi \sim 450$  MeV is at the upper border of the  $\Delta B\chi$ PT applicability. We have also performed fits with relaxed conditions  $LM_\pi \geq 3.5$  and  $r_0 M_\pi \leq 1.00$  which, however, yield equivalent results to those already presented in Table II. The present data does not allow to go below  $r_0 M_\pi \leq 1.00$ .

In Table III we summarize our results including finite-lattice spacing corrections in the fit, namely the  $c_E a^2$  and  $c_{MQ} a^2$  terms for ETMC and Mainz/QCDSF respectively. We obtain corrections of  $(+6) - (+20)$  MeV, which have an opposite sign with respect to the FV corrections. By comparing to Table II we notice that all changes are within the already given uncertainties. A noticeable qualitative effect is that changes in the Sommer-scale counterbalance finite-lattice spacing corrections so that the results are close to the former ones. A more elaborated EFT background is required to calculate and interpret finite-lattice spacing corrections more reliably.

We have tested the fits for variations of  $c_2$ ,  $c_3$  within the errors given in Table I. In all cases the results are compatible within uncertainties with those of Table II. We conclude that the  $p^4$   $B\chi$ PT fits are not able to constrain these LECs effectively. Furthermore, by varying  $c_{1\Delta}$  we find it to be correlated with  $\bar{\alpha}$ . The inclusion of  $c_{1\Delta}$  as a free parameter does not produce reliable fits unless the  $\sigma_{\pi N}(285)$  is taken into account. The fit is driven to unreasonable high  $c_{1\Delta}$  values with rather large  $\bar{\alpha}$  values. However, in fits including the  $\sigma_{\pi N}(285)$  point we recover  $c_{1\Delta} = -0.87(30) \text{ GeV}^{-1}$  together with results compatible with those in Table II. A scan over a range of  $c_{1\Delta}$  shows that reasonable fits can only be obtained in the interval  $c_{1\Delta} = -0.6 \sim -1.3 \text{ GeV}^{-1}$ . The better nucleon mass data do not allow to constrain  $c_{1\Delta}$  more accurately than the present  $\Delta$ -isobar mass lQCD data do (see Fig. 2 and the corresponding discussion).

As a final  $\sigma_{\pi N}$ -value for the  $N_f = 2$  lQCD fits we quote

$$\sigma_{\pi N} = 41(3)(1) \text{ MeV} ,$$

which corresponds to our  $p^4$   $\Delta$  and  $\Delta B\chi$ PT fits including  $\sigma_{\pi N}(285)$  and FV corrections. As for the statistical uncertainty we take larger one of  $\Delta B\chi$ PT. The difference with the result including finite spacing effects is taken as a systematic uncertainty. Note that by excluding the point  $\sigma_{\pi N}(285)$  we get a larger  $\sigma_{\pi N} = 52(13)(11) \text{ MeV}$ . This value is obtained as the average of the two  $\Delta B\chi$ PT and  $\Delta B\chi$ PT results, with the statistical uncertainty being the largest of the two errors and the second, systematic uncertainty stems from the difference between  $\Delta B\chi$ PT and

$\Delta$ B $\chi$ PT central values.

Figure 6 summarizes our results for the pion mass dependence of the  $\sigma_{\pi N}$ -term. The results for the  $\Delta$ B $\chi$ PT and  $\Delta$ B $\chi$ PT fits are compatible within errors but exhibit a different  $M_\pi$  dependence.

For our final values of the LECs  $M_0$ ,  $c_1$  and  $\bar{\alpha}$  we quote those of the  $p^4$ - $\Delta$ B $\chi$ PT fit of Tab. II including  $\sigma(285)$ . In particular, in the present work we set the Sommer-scale to  $r_0 = 0.493(23)$  fm, which is the average of all our  $p^4$  results and where the uncertainty is chosen such as to cover all our  $p^4$  fits.

### B. Nucleon mass up to order $\mathcal{O}(p^4)$ : fits to $N_f = 2 + 1$ lattice QCD data

We use our B $\chi$ PT nucleon mass formula of Eq. (18) to fit the lQCD data for the  $N_f = 2 + 1$  ensembles of Refs. [56, 58, 59, 61, 62, 89, 90]. Most of the data are provided in terms of  $(aM_\pi, aM_N)$ , together with the individual lattice spacings  $a$  and the statistical uncertainties for all the three quantities. Unlike the  $N_f = 2$  case, the available information does not allow us to perform our own scale setting. Therefore, we treat the  $a$ -uncertainties as correlated normalization errors for all  $M_N$  points from the same set. Our treatment of normalization uncertainties follows from Ref. [94]. We perform three types of fits: 1) neglecting correlated normalization errors, 2) including the normalization error in scale factors  $f_i$ , 3) including the normalization uncertainty in a correlation matrix  $V$ . For the case 3) we also consider lattice spacing effects. The  $\chi^2$  functions for type 2 and 3 fits read

$$\chi_2^2 = \sum_i \left[ \frac{M_N^{(n)}(M_\pi^2) + \Sigma_N^{(n)}(M_\pi^2, L) - f_i d_i(M_\pi^2, L)}{f_i \sigma_i} \right]^2 + \left[ \frac{f_i - 1}{\sigma_{f_i}} \right]^2, \quad (28)$$

$$\chi_3^2 = \vec{\Delta}^T V^{-1} \vec{\Delta} \quad \text{with} \quad \Delta_i = \left[ M_N^{(n)}(M_{\pi,i}^2) + c_i a_i^2 + \Sigma_N^{(n)}(M_{\pi,i}^2, L_i) - d_i(M_{\pi,i}^2, L_i) \right], \quad (29)$$

where  $M_N^{(n)}(M_\pi^2)$  and  $\Sigma_N^{(n)}(M_\pi^2, L)$  are the B $\chi$ PT continuum and finite volume expressions given in App. B4;  $d_i(M_\pi^2, L)$  are the lQCD data, each point for a given lattice size  $L$  and spacing  $a$ . We denote the statistical uncertainty for  $M_N$  coming from  $aM_N$  as  $\sigma_i$  and the normalization uncertainty coming from  $a$  as  $\sigma_{f_i}$ . Case 1) is recovered from Eq. (28) by taking all  $f_i = 1$  and replacing  $\sigma_i \rightarrow \sigma_i^2 + \sigma_{f_i}^2$  corresponding to the assumption that  $\sigma_i$  and  $\sigma_{f_i}$  are uncorrelated errors. In case 2) the  $f_i$  are additional fit parameters;  $\sigma_i^2$  and  $\sigma_{f_i}^2$  are treated separately. In case 3)  $\sigma_i^2$  and  $\sigma_{f_i}^2$  are incorporated in the correlation matrix  $V$ . The BMW collaboration [59] does not provide enough information to disentangle the uncertainties from  $aM_N$  and  $a$  so that we always include this data set with uncorrelated uncertainties.

We include in the fits data points with  $M_\pi L > 3.8$  and  $M_\pi \lesssim 415$  MeV. The LECs  $c_2$ ,  $c_3$  and  $c_{1\Delta}$  are fixed to the values given in Table I. There are two points with  $M_\pi \sim 390$  MeV from Refs. [58, 61] with very small reported  $\sigma_i$  and slightly smaller  $M_N$  values compared to the neighboring points (see Fig. 7). The inclusion of these points shifts the results to lower masses, yielding a slightly worse  $\chi^2/dof$ . Although these points were obtained by different NPLQCD and HSC Collaborations, they are not entirely independent because NPLQCD uses the scale of the HSC Collaboration, which actually expresses some concern about the quality of their lattice-spacing determination. In view of the situation, we exclude these two points from our main results but consider their influence in the systematic uncertainties.

In Table IV we display our results for the fit types 1) and 3). The results obtained with option 2) are similar to those obtained with 3) so we do not show them. The consideration of normalization uncertainties slightly enhances the  $\chi^2/dof$  but causes a noticeable reduction of  $c_1$  and  $\sigma_{\pi N}$ . The quality of the fits in terms of  $\chi^2/dof$  is essentially the same for  $p^3$  and  $p^4$  fits. As in the  $N_f = 2$  case, we expect the advantage of the  $p^4$  formula to be tangible as soon as direct  $\sigma_{\pi N}$ -data for low pion masses become available for  $N_f = 2 + 1$ .

The left panel of Fig. 7 shows the pion mass dependence of our  $\mathcal{O}(p^4)$  nucleon mass results for both  $\Delta$ B $\chi$ PT and  $\Delta$ B $\chi$ PT. There is a large overlap of the corresponding error bands, which are addressed below in more detail. By decomposing the fits into their chiral-order relative contributions (right panel of Fig. 7), we observe a similar situation as in the  $N_f = 2$  case. Namely, the  $\mathcal{O}(p^4)$  relative contributions are small over a large range of  $M_\pi$  but the  $\mathcal{O}(p^3)$  in  $\Delta$ B $\chi$ PT increases, making the applicability of our perturbative expression questionable for high  $M_\pi$  values. We have checked that a fit constrained to  $M_\pi < 360$  MeV produces results compatible with those of the  $M_\pi < 415$  MeV fit but with larger uncertainties.

The results of the fits taking into account lattice spacing effects are given in Table V. These are considered for data sets with enough points with the same  $L$  and different  $a$  values. Explicitly, we introduced two terms  $c_M a^2$  and  $c_R a^2$  for the MILC and RBCUK Collaborations, respectively. In the case of BMW, we assume that lattice spacing uncertainties are included in the errorbars. We find nucleon mass shifts of  $(-7) - (-46)$  MeV, which are small but comparable in size with the FV corrections. With this correction, the  $\chi^2/dof$  is slightly better and  $\sigma_{\pi N}$  gets smaller

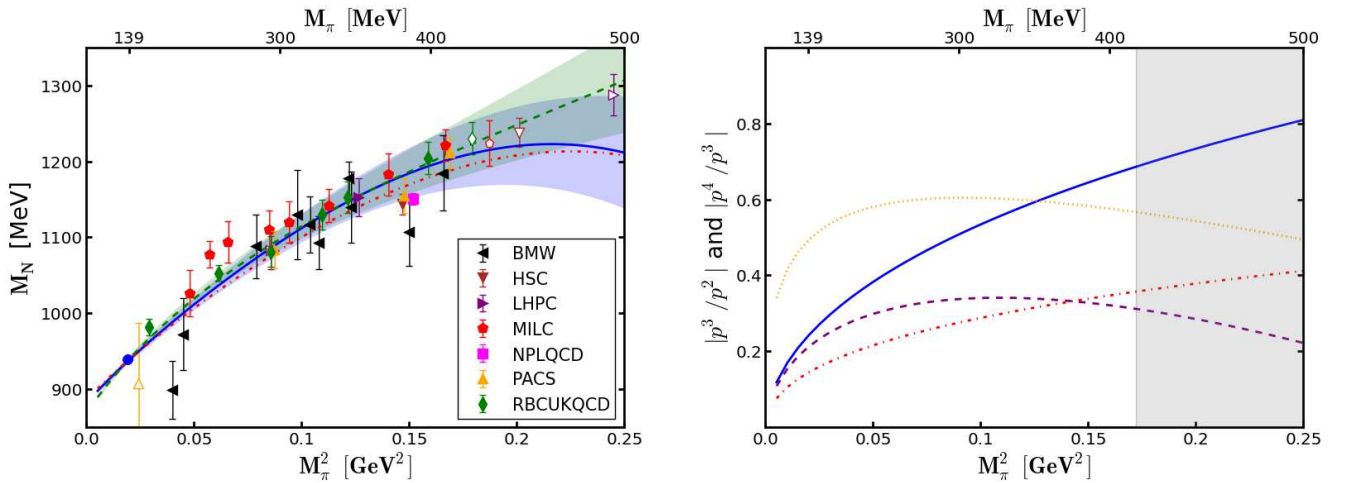


Figure 7: Combined fits to IQCD data of the  $N_f = 2 + 1$  ensembles [56, 58, 59, 61, 62, 89, 90]. Left: Fits to nucleon mass data up to  $M_\pi = 415$  MeV. The blue solid (green dashed) line shows the  $\mathcal{O}(p^4)$   $\Delta\text{B}\chi\text{PT}$  ( $\Delta\text{B}\chi\text{PT}$ ) fit of type 3). The red dotted line is also for  $\mathcal{O}(p^4)$   $\Delta\text{B}\chi\text{PT}$  but including the two points of  $M_\pi \sim 390$  MeV, excluded from the main fits as discussed in the text. Filled (open) symbols represent point included in (excluded from) the fits. Right: Decomposition of the fit results in their chiral order contributions. The blue solid line corresponds to the  $|p^3/p^2|$  ratio and the purple-dashed one to  $|p^4/p^3|$ , both for  $\Delta\text{B}\chi\text{PT}$ . The red dashed-dotted and orange-dotted are the  $|p^3/p^2|$  and  $|p^4/p^3|$  results obtained with  $\Delta\text{B}\chi\text{PT}$ .

$LM_\pi \geq 3.8$ $M_\pi \leq 415$ MeV	$\Delta\text{B}\chi\text{PT}$					$\Delta\text{B}\chi\text{PT}$				
	$M_0$ [MeV]	$c_1$ [ $\text{GeV}^{-1}$ ]	$\bar{\alpha}$ [ $\text{GeV}^{-3}$ ]	$\frac{\chi^2}{\text{dof}}$	$\sigma_\pi$ [MeV]	$M_0$ [MeV]	$c_1$ [ $\text{GeV}^{-1}$ ]	$\bar{\alpha}$ [ $\text{GeV}^{-3}$ ]	$\frac{\chi^2}{\text{dof}}$	$\sigma_\pi$ [MeV]
$p^2$	904 (2)	-0.47 (1)	-	3.1	36 (1)	-	-	-	-	-
$p^3$	883 (2)	-0.90 (1)	-	1.3	51 (1)	870 (2)	-1.10 (1)	-	1.2	60 (1)
$p^4$	870 (3)	-1.15 (3)	24 (2)	1.3	58 (3)	883 (3)	-0.89 (3)	26 (2)	1.4	49 (2)
no correl. $p^4$	865 (5)	-1.22 (5)	19 (4)	1.0	63 (3)	878 (4)	-0.96 (4)	20 (4)	1.1	54 (3)
no correl. (390) $p^4$	863 (5)	-1.25 (5)	15 (4)	1.4	64 (3)	876 (4)	-0.99 (4)	15 (3)	1.6	56 (3)

Table IV: Combined fits to the  $N_f = 2 + 1$  IQCD ensembles [56, 58, 59, 61, 62, 89, 90] for pion masses  $M_\pi \leq 415$  MeV. The LECs  $c_2$ ,  $c_3$  and  $c_{1\Delta}$  are set to the central values given in Table I; FV effects are included while  $a^2$  effects are excluded. The last two rows correspond to fits of type 1) neglecting correlated normalization errors. The fit of the last row takes into account the two points of Refs. [58, 61] with  $M_\pi \sim 390$  MeV, excluded from the main fits as discussed in the text.

by several MeV. The uncertainties for the constants  $c_M a^2$  and  $c_R a^2$  are now slightly smaller than in the 2 flavor case although all values of Tables III and V agree within the individual errors.

We tested our results for changes by varying  $c_2$ ,  $c_3$  and  $c_{1\Delta}$  within the errors quoted in Table I. All changes are within the above quoted uncertainties. In particular, changes in  $c_{1\Delta}$  are compensated by changes in  $\bar{\alpha}$  and reasonable results are only obtained for the range of  $c_{1\Delta} = (-0.5) - (-1.3)$   $\text{GeV}^{-1}$  estimated above.

As a final value for  $\sigma_{\pi N}$  in the  $N_f = 2 + 1$  case we give

$$\sigma_{\pi N} = 52 (3) (8) \text{ MeV} ,$$

obtained in the following way. The central value is the average of the four  $\mathcal{O}(p^4)$   $\Delta\text{B}\chi\text{PT}$  and  $\Delta\text{B}\chi\text{PT}$  results without (Table IV) and with (Table V) lattice spacing corrections, all including correlated normalization uncertainties. The first error correspond to the largest statistical uncertainty of the values under consideration and the second is the

	$M_0$ [MeV]	$c_1$ [ $\text{GeV}^{-1}$ ]	$\bar{\alpha}$ [ $\text{GeV}^{-3}$ ]	$c_M$ [ $\text{GeV}^{-3}$ ]	$c_R$ [ $\text{GeV}^{-3}$ ]	$\frac{\chi^2}{\text{dof}}$	$\sigma_\pi$ [MeV]
$\Delta\text{B}\chi\text{PT}$	873 (4)	-1.10 (5)	27 (3)	0.18 (8)	0.03 (2)	1.2	55 (3)
$\Delta\text{B}\chi\text{PT}$	887 (3)	-0.84 (4)	29 (3)	0.21 (8)	0.04 (2)	1.2	44 (3)

Table V: Combined fits to the  $N_f = 2 + 1$  IQCD ensembles [59, 62, 89] including  $c_a a^2$  corrections for the MILC ( $c_M$ ) and RBCUK ( $c_R$ ) Collaborations. The LECs  $c_2$ ,  $c_3$  and  $c_{1\Delta}$  are set to the central values in Table I.

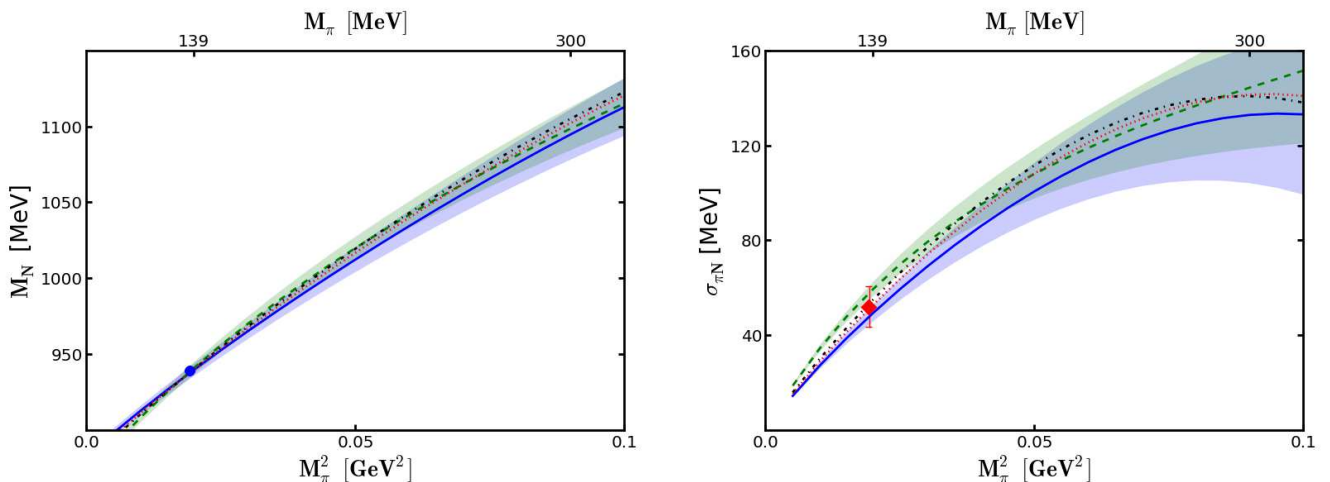


Figure 8: Pion mass dependence of  $M_N$  and  $\sigma_{\pi N}$  given by different  $\mathcal{O}(p^4)$  B $\chi$ PT fits to  $N_f = 2 + 1$  data. The blue solid and green dashed lines stand for  $\Delta$ B $\chi$ PT and  $\bar{\Delta}$ B $\chi$ PT. The red dotted line is the  $\Delta$ B $\chi$ PT solution with data points only up to 360 MeV. The black dashed-dotted line does not take correlated normalization uncertainties into account. The blue circle is the phenomenological nucleon mass and the red square is our  $\sigma_{\pi N}$  result at the physical point.

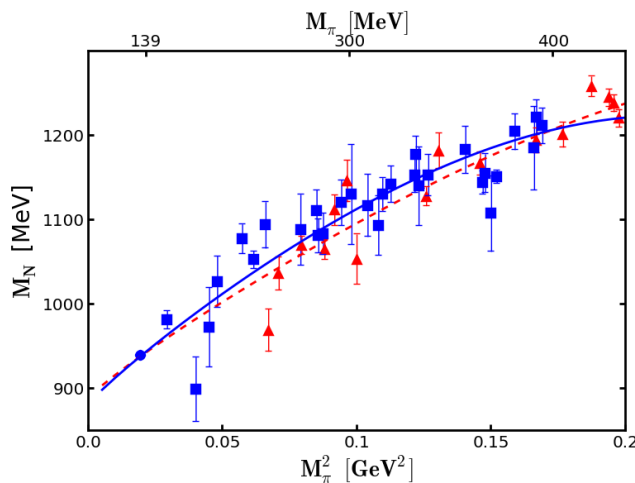


Figure 9: Pion mass dependence of the nucleon mass. The blue solid line and blue squares correspond to our fits to  $N_f = 2 + 1$  IQCD data. The red-dashed line and red-triangles correspond to our fits to  $N_f = 2$  IQCD data including the  $\sigma_{\pi N}(285)$  point. The errorbands for our fit results have been removed for the sake of clarity.

largest difference among them.

Further conclusions can be extracted from Fig. 8 where the pion mass dependence of  $M_N$  and  $\sigma_{\pi N}$  is shown for various  $p^4$  fit strategies. We can see that the small slope variations in  $M_N(M_\pi)$  (left plot) translate into changes in  $\sigma_{\pi N}$  of less than 10 MeV at the physical point (right plot). One also notices that the uncertainties of the individual IQCD data points (see Fig. V) tend to be larger than these variations. We do not expect that with more low- $M_\pi$  nucleon mass data points one would be able to reduce the  $\sigma_{\pi N}$  uncertainty much further, although simulations using one lattice action and different lattice spacings would be very important for a systematic treatment of discretization uncertainties. On the other hand,  $N_f = 2 + 1$  direct measurements of  $\sigma_{\pi N}$  at low  $M_\pi \lesssim 300$  MeV would probably lead to better constrained fits as it happens for  $N_f = 2$ , reducing uncertainties significantly.

A remarkable outcome of our analyses is the slight disagreement between the determinations of  $\sigma_{\pi N}$  using either  $N_f = 2$  or  $2 + 1$  data. Indeed, only one out of the four different  $N_f = 2 + 1$  fits used to obtain our final result is consistent with one of the  $N_f = 2$  fits. One may argue that the physical content in terms of the strange quark is different in the two types of simulations. In  $SU(2)$ -B $\chi$ PT (in the present study or in the description of  $\pi N$  scattering

data), the contribution of the strange quarks is integrated out into the LECs. For the 2-flavor ensembles, where the strange quark is quenched, one assumes that the effect of the strangeness in the nucleonic observables is negligible, whereas one includes its dynamical contributions in the  $N_f = 2 + 1$  case. Intuitively, simulations with  $2 + 1$  flavors should be closer to the real world.

However, we find it difficult to address this question with the current IQCD results, and to really tell if the observed difference could be produced, instead, by some systematic effect not properly accounted for by our analysis. In Fig. 9, we plot together the data for 2 and  $2 + 1$  flavors, as well as several fits obtained in B $\chi$ PT at  $p^4$ . The  $N_f = 2 + 1$  data are more homogeneously distributed over the low  $M_\pi$  region, where one expects the chiral extrapolators to be more reliable. For  $N_f = 2$  there is also a direct calculation of  $\sigma_{\pi N}$  in the chiral regime, which influences the fits considerably. Moreover, the scale-setting procedure is different in both cases. The physical nucleon mass was used to fix the scale in the 2-flavor case, thanks to the fact that the collaborations reported chiral-limit values for the  $r_0/a$  ratios, whereas in the  $2 + 1$  case we had to rely on independent determinations of the lattice scale and account for normalization uncertainties by incorporating correlations in the  $\chi^2$ .<sup>4</sup> In conclusion, we think our analysis exploits the considerable size of the current data set on  $M_N$  in a way that it is possible to become sensitive to unexpected systematic effects. However, more IQCD data will be required to settle this issue and interpret possible discrepancies of this type.

#### IV. SUMMARY AND CONCLUSION

We have studied the nucleon mass and the  $\sigma_{\pi N}$ -term in the  $SU(2)$  covariant B $\chi$ PT up to the chiral order  $p^4$ . We have performed fits using B $\chi$ PT with and without explicit  $\Delta$ -isobar degrees of freedom to combined IQCD data from various Collaborations for  $N_f = 2$  and  $N_f = 2 + 1$  numbers of flavors. Special attention has been paid to the different sources of uncertainties in the input data. This study is the first application of the  $p^4$   $SU(2)$  covariant B $\chi$ PT with the EOMS renormalization scheme and consistent treatment of the  $\Delta$ -isobar to IQCD data. We have included finite volume corrections and also discussed finite spacing effects. In the  $N_f = 2$  case we were able to set the IQCD data normalization via the Sommer-scale  $r_0$  and also performed simultaneous fits to nucleon mass data and one available low  $M_\pi$   $\sigma_{\pi N}$  data point. In the  $N_f = 2 + 1$  case we took into account correlated normalization uncertainties for points belonging to the same data set. In the following we summarize our findings.

- Our formula for the nucleon mass depends on several low energy constants, some of which have been fitted to the IQCD data. Explicitly, the LECs are  $M_0$ ,  $c_1$ ,  $c_2$ ,  $c_3$ ,  $c_{1\Delta}$ ,  $M_{\Delta 0}$ ,  $g_A$ ,  $f_\pi$ ,  $h_A$  and  $\bar{\alpha}$ ; the latter is a linear combination of several couplings that appear in the chiral Lagrangian at  $\mathcal{O}(p^4)$ . We adopted the phenomenological values for  $g_A$ ,  $f_\pi$  and  $h_A$ . Our fits are insensitive to the chosen values of  $c_2$ ,  $c_3$ ,  $c_{1\Delta}$  and  $M_{\Delta 0}$  so that we are not able to constrain  $c_2$  and  $c_3$  and fixed them to phenomenological values extracted in from  $\pi N$ -scattering. Furthermore, we observe that  $c_{1\Delta}$  and  $\bar{\alpha}$  are correlated, which hinders a better determination of  $c_{1\Delta}$  than the range  $c_{1\Delta} = (-0.5) - (-1.3) \text{ GeV}^{-1}$  based on rather scarce IQCD data for the  $\Delta(1232)$  mass. The LECs  $M_0$ ,  $c_1$  and  $\bar{\alpha}$  are better determined, and their values are listed in Tables II and IV for the  $N_f = 2$  and  $N_f = 2 + 1$  fits. For the  $N_f = 2$  ensembles we were able to extract the Sommer-scale, finding  $r_0 = 0.493(23) \text{ fm}$ . By performing fits to nucleon mass data alone as well as including a  $\sigma_{\pi N}$  IQCD data point at  $M_\pi = 285 \text{ MeV}$  from the QCDSF Collaboration we have obtained that the inclusion of the  $p^4$  order improves the quality of the simultaneous fits.
- For both  $N_f = 2$  and  $2 + 1$  ensembles we have investigated the effects coming from finite lattice spacings  $a$  and volumes employed in IQCD. We parametrized lattice-spacing effects by linear  $a^2$  terms. For FV we applied the standard B $\chi$ PT FV corrections. We have obtained that both effects yield comparable numerical corrections to the nucleon mass. However, we also found that the simple parametrization of the finite lattice spacing effects does not allow to disentangle it in a quantitative manner from other effects. Fit results with and without finite  $a^2$ -effects are compatible within the statistical uncertainty. In contrast to the  $a^2$ -effects, the FV corrections are very better under control by the established B $\chi$ PT techniques for the presently available IQCD volumes.
- We have extracted the  $\sigma_{\pi N}$ -term for the  $N_f = 2$  and  $N_f = 2 + 1$  IQCD ensembles obtaining  $\sigma_{\pi N} = 41(3)(1) \text{ MeV}$  and  $\sigma_{\pi N} = 52(3)(8)$ , respectively. The inclusion of the  $N_f = 2$   $\sigma_{\pi N}$  data point greatly reduces the  $\sigma_{\pi N}$  uncertainty as well as brings the two approaches,  $\Delta$ B $\chi$ PT and  $\bar{\Delta}$ B $\chi$ PT, closer. In the case of the  $N_f = 2 + 1$  ensembles, where we fitted solely nucleon mass data, the two approaches give  $\sigma_{\pi N}$ -values that differ by 9 MeV. This is a novel feature with respect to HB $\chi$ PT fits where the inclusion of the  $\Delta$ -isobar alters the result by more

---

<sup>4</sup> For a recent study of the impact of the scale fixing strategy on the value of the sigma terms see Ref. [?] ]

than 40 MeV [57]. The inclusion of finite lattice spacing correction to the  $N_f = 2 + 1$  data tends to reduce  $\sigma_{\pi N}$ . Furthermore, we want to call the attention to the fact that our result in  $N_f = 2$  is only compatible with the experimental determination based on the KA85  $\pi N$  scattering partial wave analyses of Refs [16, 37]. Our  $N_f = 2 + 1$  value is also compatible with the latest determination from the WI08 and EM06 analyses,  $\sigma_{\pi N} = 59(7)$ , which is phenomenologically favored on the grounds of consistency with  $\pi N$  phenomenology [37]. Finally, this  $N_f = 2 + 1$  result would lead, according to the traditional arguments linking sigma terms to the baryon-octet mass splittings [7, 10], to a large strangeness content in the nucleon. However, the uncertainties in these arguments have been recently revisited [95] with the conclusion that a  $\sigma_{\pi N}$  of this size is not at odds with, but favored by a negligible strangeness in the nucleon.

- With both the  $\Delta B\chi PT$  and  $\mathbb{A}B\chi PT$  approaches we obtain consistent descriptions of the pion mass dependence of the nucleon mass, as can be seen in Figs. 8 and 9. Moreover, for the current IQCD data, all our results are compatible within uncertainties and exhibit only small slope variations. However, these small variations translate into 11 MeV differences in the value of  $\sigma_{\pi N}$  at the physical point. For the 2 and 2 + 1 flavor ensembles the  $M_\pi$  distribution of the data points is different. This, together with the differences in the scale-setting procedure and the lack of low  $M_\pi$  direct  $\sigma_{\pi N}$  for  $N_f = 2 + 1$ , renders the interpretation of the 11 MeV discrepancy based on the role of strangeness difficult. To further reduce the uncertainty in the  $\sigma_{\pi N}$  value, IQCD data points with smaller uncertainties and less spread would be required. In the  $N_f = 2 + 1$  case a considerable improvement could be achieved with a direct measurement of  $\sigma_{\pi N}$  for  $M_\pi < 300$  MeV. It will be interesting to see how the  $N_f = 2$  and  $N_f = 2 + 1$  values for  $\sigma_{\pi N}$  will change when both data sets become more homogeneous.

### Acknowledgments

We thank Doug Toussaint for making the new MILC data available to us. We are also grateful to Michele Della Morte, Jambul Gegelia, Juan Nieves and Vladimir Pascalutsa for useful discussions. The work by LAR, TL and MVV has been supported by the Spanish Ministerio de Economía y Competitividad and European FEDER funds under Contracts FIS2011-28853-C02-01 and FIS2011-28853-C02-02, Generalitat Valenciana under contract PROM-ETEO/2009/0090 and the EU Hadron-Physics3 project, Grant No. 283286. JMC acknowledges support from the Science Technology and Facilities Council (STFC) under grant ST/J000477/1, the Spanish Government and FEDER funds under contract FIS2011-28853-C02-01 and the grants FPA2010-17806 and Fundación Séneca 11871/PI/09.

### Appendix A: $B\chi PT$ Lagrangians

The counting scheme of Eq. (3) defines the nucleon  $p^4$  self-energy by the sum of the graphs shown in Figs. 1. The relevant  $SU(2)$  covariant  $B\chi PT$  Lagrangians with explicit  $\Delta$ -isobar degrees of freedom are:

$$\mathcal{L}_N = \mathcal{L}_{N\pi}^{(1)} + \mathcal{L}_{N\Delta\pi}^{(1)} + \mathcal{L}_\pi^{(2)} + \mathcal{L}_{N\pi}^{(2)} + \mathcal{L}_\Delta^{(2)} + \mathcal{L}_{N\pi}^{(4)} , \quad (A1)$$

$$\mathcal{L}_\Delta = \mathcal{L}_{\Delta\pi}^{(1)} + \mathcal{L}_{N\Delta\pi}^{(1)} + \mathcal{L}_\pi^{(2)} , \quad (A2)$$

where the upper indices denote the chiral order. Explicitly, the individual isospin symmetric Lagrangians in absence of external fields and expanded in pion fields  $\pi$  are:

$$\mathcal{L}_{N\pi}^{(1)} = \bar{N} \left[ i\partial - M_0 + \frac{1}{4f_{\pi 0}^2} \epsilon^{abc} (\partial\pi^a) \pi^b \tau^c - \frac{g_{A0}}{2f_{\pi 0}} \gamma^\mu \gamma^5 (\partial_\mu \pi^a) \tau^a \right] N , \quad (A3)$$

$$\mathcal{L}_{\Delta\pi}^{(1)} = \bar{\Delta}_\mu (\gamma^{\mu\nu\alpha} i\partial_\alpha - M_{\Delta 0} \gamma^{\mu\nu}) \Delta_\nu + \frac{H_A}{2f_{\pi 0} M_{\Delta 0}} \epsilon^{\mu\nu\alpha\lambda} \bar{\Delta}_\mu \mathcal{T}^a (\partial_\alpha \Delta_\nu) \partial_\lambda \pi^a , \quad (A4)$$

$$\mathcal{L}_{\Delta N\pi}^{(1)} = i \frac{h_A}{2f_{\pi 0} M_{\Delta 0}} \bar{N} T^a \gamma^{\mu\nu\lambda} (\partial_\mu \Delta_\nu) \partial_\lambda \pi^a + \text{H.c.} , \quad (A5)$$

$$\mathcal{L}_\pi^{(2)} = \frac{1}{2} (\partial_\mu \pi^a) (\partial^\mu \pi^a) - \frac{1}{2} M^2 \pi^2 , \quad (A6)$$

$$\begin{aligned} \mathcal{L}_{N\pi}^{(2)} = & c_1 2m_\pi^2 \left[ 2 - \frac{1}{f_{\pi 0}^2} \pi^2 \right] \bar{N} N - \frac{c_2}{M_0^2 f_{\pi 0}^2} \bar{N} (\partial_\mu \pi^a) (\partial_\nu \pi^a) \partial^\mu \partial^\nu N , \\ & + \frac{c_3}{f_{\pi 0}^2} (\partial_\mu \pi^a) (\partial^\mu \pi^a) \bar{N} N - \frac{c_4}{4f_{\pi 0}^2} \bar{N} \gamma^\mu \gamma^\nu [\partial_\mu \vec{\pi}, \partial_\nu \vec{\pi}] N + c_5 \frac{m_\pi^2}{f_{\pi 0}^2} \bar{N} \left[ \pi^2 - (\vec{\pi} \cdot \vec{\tau})^2 \right] N , \end{aligned} \quad (A7)$$

$$\mathcal{L}_{\Delta}^{(2)} = 4c_{1\Delta}m_{\pi}^2\overline{\Delta}_{\mu}\gamma^{\mu\nu}\Delta_{\nu} \quad , \quad (\text{A8})$$

$$\mathcal{L}_{N\pi}^{(4)} = -\frac{1}{2}\alpha m_{\pi}^4\overline{N}N \quad , \quad (\text{A9})$$

where  $m_{\pi}^2$  is the  $\mathcal{O}(p^2)$  pion mass  $m_{\pi}^2 = 2B\overline{m}$  proportional to the chiral condensate  $B$  and the current-quark mass average  $\overline{m}$ . The Lagrangians  $\mathcal{L}_{N\pi}^{(1,2,4)}$  for the nucleon field  $N$  are those of [96] with  $\alpha = -4[8e_{38} + e_{115} + e_{116}]$  a combination of  $\mathcal{L}_{N\pi}^{(4)}$  low energy constants; the  $\mathcal{L}_{N\pi}^{(3)}$  does not produce any nucleon self-energy vertices. The couplings of the  $\Delta$ -isobar are chosen to be consistent with the covariant construct of the free Rarita-Schwinger theory and hence do not contain the unphysical degrees of freedom of vector-spinor fields. The  $\Delta$ -isobar Lagrangians and further details can be found in [34–36, 45, 97]. There are 13 low energy constants  $f_{\pi 0}, g_{A0}, c_1, c_2, c_3, c_4, c_5, H_{A0}, h_{A0}, M_0, M_{\Delta 0}, c_{1\Delta}, \alpha$  where  $c_4$  and  $c_5$  do not contribute to the nucleon mass.

The loop graphs in Fig. 1 are divergent in 4 dimensions and need to be regularized. For that we use the dimensional regularization with  $D = 4 - 2\epsilon$  dimensions and renormalize contributions proportional to:

$$L = -\frac{1}{\epsilon} - 1 + \gamma_E - \ln 4\pi \quad .$$

For the  $D$ -dimensional spin-3/2 propagator we use:

$$S_{\Delta}^{\alpha\beta}(p) = \frac{\not{p} + M_{\Delta}}{p^2 - M_{\Delta}^2 + i\epsilon} \left[ -g^{\alpha\beta} + \frac{1}{D-1}\gamma^{\alpha}\gamma^{\beta} + \frac{1}{(D-1)M_{\Delta}}(\gamma^{\alpha}p^{\beta} - \gamma^{\beta}p^{\alpha}) + \frac{D-2}{(D-1)M_{\Delta}^2}p^{\alpha}p^{\beta} \right] .$$

The appearing totally anti-symmetric  $\gamma$ -matrices are:

$$\begin{aligned} \gamma^{\mu\nu} &= \frac{1}{2}[\gamma^{\mu}, \gamma^{\nu}] \quad , \\ \gamma^{\mu\nu\rho} &= \frac{1}{2}\{\gamma^{\mu\nu}, \gamma^{\rho}\} = i\varepsilon^{\mu\nu\rho\sigma}\gamma_5\gamma_{\sigma} = \gamma^{\mu\nu\rho\sigma}\gamma_5 \quad , \\ \gamma^{\mu\nu\rho\sigma} &= \frac{1}{2}[\gamma^{\mu\nu\rho}, \gamma^{\sigma}] = i\varepsilon^{\mu\nu\rho\sigma}\gamma_5 \quad . \end{aligned}$$

## Appendix B: Self-energy formulas

### 1. Nucleon self-energies

For the nucleon mass we need the self-energy expressions corresponding to the Feynman-graphs in Fig. 1. The contributions listed in increasing chiral order are:

$$\begin{aligned} \Sigma^{(2)}(m_{\pi}^2) &= \Sigma_{C2}(m_{\pi}^2) \quad , \\ \Sigma^{(3)}(m_{\pi}^2, \not{p}) &= \Sigma_{N3}(m_{\pi}^2, \not{p}) + \Sigma_{N\Delta 3}(m_{\pi}^2, \not{p}) \quad , \\ \Sigma^{(4)}(m_{\pi}^2, \not{p}) &= \Sigma_{N4}(m_{\pi}^2, \not{p}) + \Sigma_{T4}(m_{\pi}^2, \not{p}) + \Sigma_{C4}(m_{\pi}^2, \not{p}) + \Sigma_{N\Delta 4}(m_{\pi}^2, \not{p}) \quad , \end{aligned}$$

where we keep the  $\not{p}$  dependence explicit and a ' $\Delta$ ' in the index denotes contributions from loop-internal  $\Delta$ -isobars. The individual unregularized self-energies read:

$$\Sigma_{C2}(m_{\pi}^2) = -c_{1\Delta}m_{\pi}^2 \quad (\text{B1})$$

$$\begin{aligned} \Sigma_{N3}(m_{\pi}^2, \not{p}) &= 3 \left[ \frac{g_{A0}}{8f_{\pi 0}\pi} \right]^2 \int_0^1 dz \left\{ (z\not{p} - M_0 - 2\not{p})\mathcal{M}_N^2 + (1-z)^2(\not{p})^2(z\not{p} - M_0) \left[ L + \ln \frac{\mathcal{M}_N^2}{\Lambda^2} \right] \right. \\ &\quad \left. + (-4\not{p} - 2M_0 + 3z\not{p})\mathcal{M}_N^2 \left[ L - 1 + \ln \frac{\mathcal{M}_N^2}{\Lambda^2} \right] \right\} \quad (\text{B2}) \end{aligned}$$

$$\Sigma_{N4}(m_{\pi}^2) = -c_{1\Delta}m_{\pi}^2 \frac{\partial}{\partial M_0} \Sigma_{N3}(m_{\pi}^2, \not{p}) \Big|_{\not{p}=M_0} \quad (\text{B3})$$



$$= c_1 m_\pi^2 12 \left[ \frac{g_A}{8F_\pi \pi} \right]^2 \int_0^1 dz 2(1-z) \left\{ 3\mathcal{M}_N^2 \left[ L - 1 + \ln \frac{\mathcal{M}_N^2}{\Lambda^2} \right] \right. \quad (\text{B4})$$

$$\left. + 3M_0^2 (2 - 2z + z^2) \left[ L + \ln \frac{\mathcal{M}_N^2}{\Lambda^2} \right] + \left( (1-z)^2 + 2 \right) M_0^2 + \frac{5}{2} \mathcal{M}_N^2 + \frac{(1-z)^4}{2\mathcal{M}_N^2} \right\}$$

$$\Sigma_{T4}(m_\pi^2) = \frac{3}{4F_\pi^2 (4\pi)^2} (8c_1 - c_2 - 4c_3) \left[ L - 1 + \ln \frac{m_\pi^2}{\Lambda^2} \right] m_\pi^4 + c_2 \frac{3}{8f_{\pi 0}^2 (4\pi)^2} m_\pi^4 \quad (\text{B5})$$

$$\Sigma_{C4}(m_\pi^2) = \frac{1}{2} \alpha m_\pi^4 \quad (\text{B6})$$

$$\Sigma_{N\Delta 3}(m_\pi^2, \not{p}) = \left[ \frac{h_{A0}}{8f_{\pi 0} M_{\Delta 0} \pi} \right]^2 \int_0^1 dz (z\not{p} + M_{\Delta 0}) p^2 \left\{ -2\mathcal{M}_\Delta^2 - 2\mathcal{M}_\Delta^2 \left[ L - 1 + \ln \frac{\mathcal{M}_\Delta^2}{\Lambda^2} \right] \right\} \quad (\text{B7})$$

$$\Sigma_{N\Delta 4}(m_\pi^2) = c_{1\Delta} 8m_\pi^2 \left[ \frac{h_{A0}}{8f_{\pi 0} \pi M_{\Delta 0}} \right]^2 \int_0^1 dz (1-z) M_0^2 \left\{ 3\mathcal{M}^2 \left[ L - 1 + \ln \tilde{\mathcal{M}}^2 \right] + 4\mathcal{M}^2 \right. \quad (\text{B8})$$

$$\left. + (M_{\Delta 0}^2 + 2M_0 M_{\Delta 0} z + M_0^2 z^2) \left[ L + \ln \tilde{\mathcal{M}}^2 \right] + M_{\Delta 0}^2 + 2M_0 M_{\Delta 0} z + M_0^2 z^2 \right\} ,$$

with the expression

$$\mathcal{M}_N^2 = z m_\pi^2 - z(1-z)p^2 + (1-z)M_0^2 , \quad (\text{B9})$$

$$\mathcal{M}_\Delta^2 = z m_\pi^2 - z(1-z)p^2 + (1-z)M_{\Delta 0}^2 . \quad (\text{B10})$$

## 2. $\Delta(1232)$ self-energies

In Sec. IIB we use the pion mass dependence of the  $\Delta$ -isobar to constrain the LEC  $c_{1\Delta}$ . The  $\Delta$ -isobar mass to order  $p^3$  is

$$M_\Delta^{(3)}(m_\pi^2) = M_{\Delta 0} + \Sigma_{\Delta 2}(m_\pi^2) + \Sigma_{\Delta N 3}(m_\pi^2) + \Sigma_{\Delta \Delta 3}(m_\pi^2) , \quad (\text{B11})$$

where the self-energies are defined as

$$\Sigma_\Delta^{\alpha\beta}(\not{p}) = -g^{\alpha\beta} [\not{p}\Sigma_\Delta^A(M_{\Delta 0}) + \Sigma_\Delta^B(M_{\Delta 0})] , \quad (\text{B12})$$

with the unregularized expressions

$$\Sigma_{C\Delta 2}(m_\pi^2) = -c_{1\Delta} 4m_\pi^2 , \quad (\text{B13})$$

$$\Sigma_{\Delta N 3}(m_\pi^2) = -\frac{1}{2} \left[ \frac{h_A}{8f_{\pi 0} \pi} \right]^2 \int_0^1 dz \left\{ (zM_{\Delta 0} + M_0) \mathcal{M}_{\Delta N}^2 \left[ L - 1 + \ln \frac{\mathcal{M}_{\Delta N}^2}{\Lambda^2} \right] + 4(zM_{\Delta 0} + M_{N0}) \mathcal{M}_{\Delta N}^2 \right\} \quad (\text{B14})$$

$$\mathcal{M}_{\Delta N}^2 = z m_\pi^2 - z(1-z)M_{\Delta 0}^2 + (1-z)M_0^2 , \quad (\text{B15})$$

$$\Sigma_{\Delta \Delta 3}(m_\pi^2) = -\frac{5}{3} \left[ \frac{H_A}{8f_{\pi 0} \pi} \right]^2 \int_0^1 dz \left\{ \frac{5}{6} M_{\Delta 0} (1+z) \mathcal{M}_{\Delta \Delta}^2 \left[ L - 1 + \ln \frac{\mathcal{M}_{\Delta \Delta}^2}{\Lambda^2} \right] + \frac{13}{9} M_{\Delta 0} (1+z) \mathcal{M}_{\Delta \Delta}^2 \right\} , \quad (\text{B16})$$

$$\mathcal{M}_{\Delta \Delta}^2 = z m_\pi^2 - z(1-z)M_{\Delta 0}^2 + (1-z)M_0^2 . \quad (\text{B17})$$

These contributions are the  $\Delta$ -isobar versions of the nucleon graphs  $\Sigma_{C2}$ ,  $\Sigma_{N3}$  and  $\Sigma_{N\Delta 3}$  of Fig. 1. The  $\Sigma_{C\Delta 2}$  is the  $\Delta$ -isobar contact graph and the  $\Sigma_{\Delta N 3}$  and  $\Sigma_{\Delta \Delta 3}$  are  $p^3$  loop with external  $\Delta$ -isobars and an internal nucleon and  $\Delta$ -isobar, respectively.

## 3. Finite volume corrections to the nucleon self-energies

The loop graphs  $\Sigma_{N3}$ ,  $\Sigma_{N4}$ ,  $\Sigma_{T4}$  and  $\Sigma_{N\Delta 3}$ ,  $\Sigma_{N\Delta 4}$  of Fig. 1 are subject to finite volume (FV) effects when the nucleon is placed in a discretized box. We calculate these effects by the standard techniques of [43]. In the following

we summarize the calculation of the loop-integral with a single propagator and list afterwards all appearing FV corrections for the nucleon mass to order  $p^4$ .

For the FV calculation we chose the nucleon rest-frame  $\not{p} = \gamma_0 p_0 = \gamma_0 M_N$ . As a consequence all appearing loop-integrals can be brought into the form of

$$\int \frac{d^4 l}{(2\pi)^4} \frac{l \cdot A l \cdot B \dots}{l^2 - m^2} \rightarrow \int \frac{d^4 l}{(2\pi)^4} \frac{l_0^a}{l^2 - m^2} , \quad (\text{B18})$$

where no Lorentz-decomposition has to be used,  $A$  and  $B$  are given 4-vectors and  $a$  a power of the 0th-loop momentum component. The loop-momentum  $l$  is now discretized with respect to the box size  $L$  by

$$\int \frac{d^4 l}{(4\pi)^4} = \int \frac{dl_0}{2\pi} \frac{d\vec{l}}{(2\pi)^3} \rightarrow \int \frac{dl_0}{2\pi} \frac{1}{L^3} \sum_{\vec{n}} \quad \text{with } \vec{l} = \frac{2\pi}{L} \vec{n} \quad \vec{n} \in \mathbb{Z}^3 , \quad (\text{B19})$$

such that after Wick-rotating and the use of Poisson's formula we get:

$$\int \frac{dl_0}{2\pi} \frac{1}{L^3} \sum_{\vec{n}} \frac{l_0^a}{l_0^2 - \frac{2\pi}{L} \vec{n}^2 - m^2} = -i^{\alpha+1} \int_{-\infty}^{\infty} \frac{dl_4}{2\pi} \int_{-\infty}^{\infty} \frac{d\vec{l}}{(2\pi)^3} \frac{l_4^a}{l_4^2 + \vec{l}^2 + m^2} \frac{(2\pi)^3}{L^3} \sum_{\vec{n}} \delta^{(3)} \left( \vec{l} - \frac{2\pi}{L} \vec{n}^2 \right) \quad (\text{B20})$$

$$= -i^{\alpha+1} \int_{-\infty}^{\infty} \frac{dl_4}{2\pi} \int_{-\infty}^{\infty} \frac{d\vec{l}}{(2\pi)^3} \frac{l_4^a}{l_4^2 + \vec{l}^2 + m^2} \sum_{\vec{j}} e^{iL\vec{j}\cdot\vec{l}} , \quad (\text{B21})$$

with  $\vec{j} \in \mathbb{Z}^3$ . The case  $\vec{j} = 0$  corresponds to the usual continuum result whereas the cases  $\vec{j} \neq 0$  are the finite volume corrections. All remaining integrals can be solved analytically. For our nucleon mass expression we need the following solutions:

$$\int \frac{d^4 l}{(2\pi)^4} \frac{1}{l^2 - m^2} = \frac{-i}{(4\pi)^2} \sum_{\vec{j} \neq 0} 4 \frac{\sqrt{m^2}}{Lj} K_1(F) , \quad \int \frac{d^4 l}{(2\pi)^4} \frac{l_0^2}{l^2 - m^2} = \frac{-i}{(4\pi)^2} \sum_{\vec{j} \neq 0} \frac{(-4)m^2}{(Lj)^2} K_2(F) , \quad (\text{B22})$$

$$\int \frac{d^4 l}{(2\pi)^4} \frac{1}{[l^2 - m^2]^2} = \frac{-i}{(4\pi)^2} \sum_{\vec{j} \neq 0} (-2) K_0(F) , \quad \int \frac{d^4 l}{(2\pi)^4} \frac{l_0^2}{[l^2 - m^2]^2} = \frac{-i}{(4\pi)^2} \sum_{\vec{j} \neq 0} 2 \frac{\sqrt{m^2}}{Lj} K_1(F) , \quad (\text{B23})$$

$$\int \frac{d^4 l}{(2\pi)^4} \frac{1}{[l^2 - m^2]^3} = \frac{-i}{(4\pi)^2} \sum_{\vec{j} \neq 0} \frac{1}{2} \frac{Lj}{\sqrt{m^2}} K_1(F) , \quad \int \frac{d^4 l}{(2\pi)^4} \frac{l_0^2}{[l^2 - m^2]^3} = \frac{-i}{(4\pi)^2} \sum_{\vec{j} \neq 0} \left( -\frac{1}{2} \right) K_0(F) , \quad (\text{B24})$$

where the  $K_\nu(x)$  are modified Bessel-functions of the second kind with  $F = Lj\sqrt{m^2}$  and  $j = \sqrt{j_x^2 + j_y^2 + j_z^2}$  with  $j_i \in \mathbb{Z}$ .

To collect our final results we use the notations:

$$F_N = Lj\sqrt{\mathcal{M}_N^2} , \quad \Sigma'_{N3}(m_\pi^2, L) = \left. \frac{\partial}{\partial p_0} \Sigma_{N3}(p_0, m_\pi^2, L) \right|_{p_0=M_0} , \quad (\text{B25})$$

$$F_\Delta = Lj\sqrt{\mathcal{M}_\Delta^2} , \quad \Sigma'_{N\Delta 3}(m_\pi^2, L) = \left. \frac{\partial}{\partial p_0} \Sigma_{N\Delta 3}(p_0, m_\pi^2, L) \right|_{p_0=M_0} , \quad (\text{B26})$$

where the arguments of the self-energies distinguish them from their continuum counterparts.

The individual finite volume contributions corresponding to the loop-graphs in Fig. 1 are:

$$\Sigma_{N3}(m_\pi^2, L) = 3 \left[ \frac{g_A}{8f_\pi\pi} \right]^2 \sum_{\vec{j} \neq 0} \int_0^1 dz 2M_0 \left[ \begin{aligned} & \left( (1-z)^3 M_0^2 + (3-z) \mathcal{M}^2 \right) K_0(F_N) + (4z-6) \frac{\sqrt{\mathcal{M}^2}}{Lj} K_1(F_N) \end{aligned} \right] \quad (\text{B27})$$

$$\begin{aligned} \Sigma'_{N3}(m_\pi^2, L) = & 3 \left[ \frac{g_A}{8f_\pi\pi} \right]^2 \sum_{\vec{j} \neq 0} \int_0^1 dz \left[ 4 \left[ + (2z-2) \frac{\sqrt{\mathcal{M}^2}}{Lj} K_1(F_N) \right. \right. \\ & - \frac{1}{2} \left. \left. \left( (z-2) \mathcal{M}^2 + M_0^2 (1-z) \left[ (1-z)(3z-2) - 2z^2 - 4z(z-3) \right] \right) K_0(F_N) \right. \right. \\ & \left. \left. + \frac{1}{2} z (1-z) M_0^2 \left( (1-z)^3 M_0^2 + (3-z) \mathcal{M}^2 \right) \frac{Lj}{\sqrt{\mathcal{M}_N^2}} K_1(F_N) \right] \right] \end{aligned} \quad (\text{B28})$$

$$\begin{aligned} \Sigma_{N4}(m_\pi^2, L) = & -c_{14} m_\pi^2 3 \left[ \frac{g_A}{8f_\pi\pi} \right]^2 \int_0^1 dz \sum_{\vec{j} \neq 0} \left[ \right. \\ & + 2 \left( \mathcal{M}_N^2 + (1-z)^2 M_0^2 - 2z(1-z) M_0^2 - 4(1-z)(z-3) M_0^2 \right) K_0(F_N) \\ & \left. + 2M_0^2 (1-z) \left( (z-3) \mathcal{M}_N^2 - (1-z)^3 M_0^2 \right) \frac{Lj}{\sqrt{\mathcal{M}_N^2}} K_1(F_N) - 4 \frac{\sqrt{\mathcal{M}_N^2}}{Lj} K_1(F_N) \right] \end{aligned} \quad (\text{B29})$$

$$\begin{aligned} \Sigma_{T4}(m_\pi^2, L) = & \frac{12m_\pi^2}{F_\pi^2 (4\pi)^2} \sum_{\vec{j} \neq 0} \\ & \left[ 2c_1 \frac{\sqrt{m_\pi^2}}{Lj} K_1(Lj\sqrt{m_\pi^2}) + c_2 \frac{1}{(Lj)^2} K_2(Lj\sqrt{m_\pi^2}) - c_3 \frac{\sqrt{m_\pi^2}}{Lj} K_1(Lj\sqrt{m_\pi^2}) \right] \end{aligned} \quad (\text{B30})$$

$$\begin{aligned} \Sigma_{N\Delta 3}(m_\pi^2, L) = & \frac{4}{3} \left[ \frac{h_A}{8f_\pi\pi M_{\Delta 0}} \right]^2 \int_0^1 dz (zM_0 + M_{\Delta 0}) 2M_0^2 \\ & \left[ - \frac{\sqrt{\mathcal{M}_\Delta^2}}{Lj} K_1(Lj\sqrt{\mathcal{M}_\Delta^2}) + \mathcal{M}_\Delta^2 K_0(Lj\sqrt{\mathcal{M}_\Delta^2}) \right] \end{aligned} \quad (\text{B31})$$

$$\begin{aligned} \Sigma'_{N\Delta 3}(m_\pi^2, L) = & \frac{4}{3} \left[ \frac{h_A}{8f_\pi M_{\Delta 0} \pi} \right]^2 \int_0^1 dz \left[ 2z(1-z) M_0^3 (zM_0 + M_{\Delta 0}) \mathcal{M}_\Delta^2 \frac{Lj}{\sqrt{\mathcal{M}_\Delta^2}} K_1(F_\Delta) \right. \\ & - 2M_0 (3zM_0 + 2M_{\Delta 0}) \frac{\sqrt{\mathcal{M}_\Delta^2}}{Lj} K_1(F_\Delta) \\ & \left. + (-6z(1-z) M_0^3 (zM_0 + M_{\Delta 0}) + 2M_0 (3zM_0 + 2M_{\Delta 0}) \mathcal{M}_\Delta^2) K_0(F_\Delta) \right] \end{aligned} \quad (\text{B32})$$

$$\begin{aligned} \Sigma_{N\Delta 4}(m_\pi^2, L) = & c_{1\Delta} 4m_\pi^2 2 \left[ \frac{h_A}{8f_\pi\pi M_{\Delta 0}} \right]^2 \int_0^1 dz 2(1-z) \frac{1}{3} M_0^2 \left[ \right. \\ & - (3z^2 M_0^2 + 3M_{\Delta 0}^2 + 6zM_0 M_{\Delta 0} + 7\mathcal{M}_\Delta^2) K_0(F_\Delta) \\ & \left. + 4 \frac{\sqrt{\mathcal{M}_\Delta^2}}{Lj} K_1(F_\Delta) + \mathcal{M}_\Delta^2 (z^2 M_0^2 + M_{\Delta 0}^2 + 2zM_0 M_{\Delta 0} + \mathcal{M}_\Delta^2) \frac{Lj}{\sqrt{\mathcal{M}_\Delta^2}} K_1(F_\Delta) \right] . \end{aligned} \quad (\text{B33})$$

#### 4. Fit formulas

In Secs. III A and III B we use in the  $\chi^2$  fits the following nucleon mass expressions:

$$M_N^{(2)}(M_\pi^2) = M_0 + \Sigma_{C2}(M_\pi^2) , \quad (\text{B34})$$

$$M_N^{(3)}(M_\pi^2) = M_0 + \Sigma_{C2}(M_\pi^2) + \Sigma_{N3}(M_\pi^2) , \quad (\text{B35})$$

$$M_N^{(3\Delta)}(M_\pi^2) = M_0 + \Sigma_{C2}(M_\pi^2) + \Sigma_{N3}(M_\pi^2) + \Sigma_{N\Delta 3}(M_\pi^2) , \quad (\text{B36})$$

$$\begin{aligned} M_N^{(4)}(M_\pi^2) = & M_0 + \Sigma_{C2}(M_\pi^2) + \Sigma_{N3}(M_\pi^2) + \Sigma_{N4}(M_\pi^2) + \Sigma_{T4}(M_\pi^2) \\ & + \frac{1}{2} \alpha M_\pi^4 + \Sigma_{C2}(M_\pi^2) \Sigma'_{N3}(M_\pi^2) + \frac{c_1}{8\pi^2 f_\pi^2} M_\pi^4 \ln \frac{M_\pi^2}{M_N^2} , \end{aligned} \quad (\text{B37})$$

$$M_N^{(4\Delta)}(M_\pi^2) = M_0 + \Sigma_{C2}(M_\pi^2) + \Sigma_{N3}(M_\pi^2) + \Sigma_{N4}(M_\pi^2) + \Sigma_{T4}(M_\pi^2)$$

$$\begin{aligned}
& + \frac{1}{2} \bar{\alpha} M_\pi^4 + \Sigma_{C2} (M_\pi^2) \Sigma'_{N3} (M_\pi^2) + \frac{c_1}{8\pi^2 f_\pi^2} M_\pi^4 \ln \frac{M_\pi^2}{M_N^2} \\
& + \Sigma_{N\Delta3} (M_\pi^2) + \Sigma_{N\Delta4} (M_\pi^2) + \Sigma_{C2} (M_\pi^2) \Sigma'_{N\Delta3} (M_\pi^2) \quad , \quad (B38)
\end{aligned}$$

where all loops are evaluated at  $\not{p} = M_0$ . The additional terms proportional to  $c_1$ , as compared to Eq. (13), come from the discussion in Sec. II B. In the case of fits with finite volume corrections, we add the following expressions:

$$\Sigma_{FV}^{(3)} (M_\pi^2, L) = \Sigma_{N3} (M_\pi^2, L) \quad (B39)$$

$$\Sigma_{FV}^{(3\Delta)} (M_\pi^2, L) = \Sigma_{N3} (M_\pi^2, L) + \Sigma_{N\Delta3} (M_\pi^2, L) \quad (B40)$$

$$\Sigma_{FV}^{(4)} (M_\pi^2, L) = \Sigma_{N3} (M_\pi^2, L) + \Sigma_{N4} (M_\pi^2, L) + \Sigma_{T4} (M_\pi^2, L) + \Sigma_{C2} (M_\pi^2) \Sigma'_{N3} (M_\pi^2, L) \quad (B41)$$

$$\begin{aligned}
\Sigma_{FV}^{(4\Delta)} (M_\pi^2, L) &= \Sigma_{N3} (M_\pi^2, L) + \Sigma_{N\Delta3} (M_\pi^2, L) \\
&+ \Sigma_{N4} (M_\pi^2, L) + \Sigma_{N\Delta4} (M_\pi^2, L) + \Sigma_{T4} (M_\pi^2, L) \\
&+ \Sigma_{C2} (M_\pi^2) \Sigma'_{N3} (M_\pi^2, L) + \Sigma_{C2} (M_\pi^2) \Sigma'_{N\Delta3} (M_\pi^2, L) \quad (B42)
\end{aligned}$$

- [1] S. Weinberg, *Physica* **A96**, 327 (1979).
- [2] J. Gasser and H. Leutwyler, *Annals Phys.* **158**, 142 (1984).
- [3] J. Gasser, M. Sainio, and A. Svarc, *Nucl.Phys.* **B307**, 779 (1988).
- [4] H. Leutwyler, *Ann. Phys.* **235**, 165 (1994), hep-ph/9311274.
- [5] Z. Fodor and C. Hoelbling, *Rev.Mod.Phys.* **84**, 449 (2012), 1203.4789.
- [6] E. E. Jenkins and A. V. Manohar, *Phys.Lett.* **B255**, 558 (1991).
- [7] B. Borasoy and U.-G. Meissner, *Annals Phys.* **254**, 192 (1997), hep-ph/9607432.
- [8] H. Hellmann, *Z.Phys.A* **85**, 180 (1933).
- [9] R. P. Feynman, *Phys. Rev.* **56**, 340 (1939).
- [10] J. Gasser, *Annals Phys.* **136**, 62 (1981).
- [11] A. Bottino, F. Donato, N. Fornengo, and S. Scopel, *Astropart.Phys.* **18**, 205 (2002), hep-ph/0111229.
- [12] A. Bottino, F. Donato, N. Fornengo, and S. Scopel, *Phys.Rev.* **D78**, 083520 (2008), 0806.4099.
- [13] J. R. Ellis, K. A. Olive, and C. Savage, *Phys.Rev.* **D77**, 065026 (2008), 0801.3656.
- [14] T. Cheng and R. F. Dashen, *Phys.Rev.Lett.* **26**, 594 (1971).
- [15] R. Koch, *Z.Phys.* **C15**, 161 (1982).
- [16] J. Gasser, H. Leutwyler, and M. Sainio, *Phys.Lett.* **B253**, 252 (1991).
- [17] M. Olsson, *Phys.Lett.* **B482**, 50 (2000), hep-ph/0001203.
- [18] M. Pavan, I. Strakovsky, R. Workman, and R. Arndt, *PiN Newslett.* **16**, 110 (2002), hep-ph/0111066.
- [19] G. E. Hite, W. B. Kaufmann, and R. J. Jacob, *Phys.Rev.* **C71**, 065201 (2005).
- [20] J. Stahov, H. Clement, and G. Wagner (2012), 1211.1148.
- [21] J. Gasser, H. Leutwyler, and M. Sainio, *Phys.Lett.* **B253**, 260 (1991).
- [22] T. Becher and H. Leutwyler, *Eur.Phys.J.* **C9**, 643 (1999), hep-ph/9901384.
- [23] J. Gegelia and G. Japaridze, *Phys.Rev.* **D60**, 114038 (1999), hep-ph/9908377.
- [24] T. Fuchs, J. Gegelia, G. Japaridze, and S. Scherer, *Phys.Rev.* **D68**, 056005 (2003), hep-ph/0302117.
- [25] P. Buettiker and U.-G. Meissner, *Nucl.Phys.* **A668**, 97 (2000), hep-ph/9908247.
- [26] B. R. Holstein, V. Pascalutsa, and M. Vanderhaeghen, *Phys.Rev.* **D72**, 094014 (2005), hep-ph/0507016.
- [27] L. Geng, J. Martin Camalich, L. Alvarez-Ruso, and M. Vicente Vacas, *Phys.Rev.Lett.* **101**, 222002 (2008), 0805.1419.
- [28] T. Becher and H. Leutwyler, *JHEP* **0106**, 017 (2001), hep-ph/0103263.
- [29] J. Alarcon, J. M. Camalich, and J. Oller (2012), 1210.4450.
- [30] Y.-H. Chen, D.-L. Yao, and H. Zheng (2012), 1212.1893.
- [31] T. R. Hemmert, B. R. Holstein, and J. Kambor, *Phys.Lett.* **B395**, 89 (1997), hep-ph/9606456.
- [32] T. R. Hemmert, B. R. Holstein, and J. Kambor, *J.Phys.* **G24**, 1831 (1998), hep-ph/9712496.
- [33] V. Pascalutsa and D. R. Phillips, *Phys.Rev.* **C67**, 055202 (2003), nucl-th/0212024.
- [34] V. Pascalutsa and R. Timmermans, *Phys.Rev.* **C60**, 042201 (1999), nucl-th/9905065.
- [35] V. Pascalutsa, *Phys.Lett.* **B503**, 85 (2001), hep-ph/0008026.
- [36] V. Pascalutsa, M. Vanderhaeghen, and S. N. Yang, *Phys.Rept.* **437**, 125 (2007), hep-ph/0609004.
- [37] J. Alarcon, J. Martin Camalich, and J. Oller, *Phys.Rev.* **D85**, 051503 (2012), 1110.3797.
- [38] S. Dinter et al. (ETM Collaboration), *JHEP* **1208**, 037 (2012), 1202.1480.
- [39] D. B. Leinweber, A. W. Thomas, and S. V. Wright, *Phys.Lett.* **B482**, 109 (2000), hep-lat/0001007.
- [40] D. B. Leinweber, A. W. Thomas, and R. D. Young, *Phys.Rev.Lett.* **92**, 242002 (2004), hep-lat/0302020.
- [41] V. Bernard, T. R. Hemmert, and U.-G. Meissner, *Nucl.Phys.* **A732**, 149 (2004), hep-ph/0307115.
- [42] M. Procura, T. R. Hemmert, and W. Weise, *Phys.Rev.* **D69**, 034505 (2004), hep-lat/0309020.

- [43] A. Ali Khan et al. (QCDSF-UKQCD Collaboration), Nucl.Phys. **B689**, 175 (2004), hep-lat/0312030.
- [44] M. Procura, B. Musch, T. Wollenweber, T. Hemmert, and W. Weise, Phys.Rev. **D73**, 114510 (2006), hep-lat/0603001.
- [45] V. Pascalutsa and M. Vanderhaeghen, Phys.Lett. **B636**, 31 (2006), hep-ph/0511261.
- [46] C. Alexandrou et al. (European Twisted Mass Collaboration), Phys.Rev. **D78**, 014509 (2008), 0803.3190.
- [47] H. Ohki, H. Fukaya, S. Hashimoto, T. Kaneko, H. Matsufuru, et al., Phys.Rev. **D78**, 054502 (2008), 0806.4744.
- [48] G. Bali, P. Bruns, S. Collins, M. Deka, B. Glasle, et al., Nucl.Phys. **B866**, 1 (2013), 1206.7034.
- [49] A. Chowdhury, A. K. De, S. De Sarkar, A. Harindranath, J. Maiti, et al. (2012), 1212.0717.
- [50] G. S. Bali et al. (QCDSF Collaboration), Phys.Rev. **D85**, 054502 (2012), 1111.1600.
- [51] C. Alexandrou, K. Hadjiyiannakou, G. Koutsou, A. O’Cais, and A. Strelchenko, Comput.Phys.Commun. **183**, 1215 (2012), 1108.2473.
- [52] C. W. Bernard, T. Burch, K. Orginos, D. Toussaint, T. A. DeGrand, et al., Phys.Rev. **D64**, 054506 (2001), hep-lat/0104002.
- [53] C. Aubin, C. Bernard, C. DeTar, J. Osborn, S. Gottlieb, et al., Phys.Rev. **D70**, 094505 (2004), hep-lat/0402030.
- [54] C. Bernard et al. (MILC Collaboration), PoS **LAT2007**, 137 (2007), 0711.0021.
- [55] S. Durr, Z. Fodor, J. Frison, C. Hoelbling, R. Hoffmann, et al., Science **322**, 1224 (2008), 0906.3599.
- [56] S. Aoki et al. (PACS-CS Collaboration), Phys.Rev. **D79**, 034503 (2009), 0807.1661.
- [57] A. Walker-Loud, PoS **LATTICE2008**, 005 (2008), 0810.0663.
- [58] H.-W. Lin et al. (Hadron Spectrum Collaboration), Phys.Rev. **D79**, 034502 (2009), 0810.3588.
- [59] S. Durr, Z. Fodor, T. Hemmert, C. Hoelbling, J. Frison, et al., Phys.Rev. **D85**, 014509 (2012), 1109.4265.
- [60] W. Bietenholz, V. Bornyakov, M. Gockeler, R. Horsley, W. Lockhart, et al., Phys.Rev. **D84**, 054509 (2011), 1102.5300.
- [61] S. Beane, E. Chang, W. Detmold, H. Lin, T. Luu, et al., Phys.Rev. **D84**, 014507 (2011), 1104.4101.
- [62] C. Jung (RBC Collaboration, UKQCD Collaboration), PoS **LATTICE2012**, 164 (2012), 1301.5397.
- [63] K.-I. Ishikawa et al. (PACS-CS Collaboration), Phys.Rev. **D80**, 054502 (2009), 0905.0962.
- [64] R. Young and A. Thomas, Phys.Rev. **D81**, 014503 (2010), 0901.3310.
- [65] P. Shanahan, A. Thomas, and R. Young (2012), 1205.5365.
- [66] A. Semke and M. Lutz, Nucl.Phys. **A789**, 251 (2007), nucl-th/0606027.
- [67] J. Martin Camalich, L. Geng, and M. Vicente Vacas, Phys.Rev. **D82**, 074504 (2010), 1003.1929.
- [68] L.-s. Geng, X.-l. Ren, J. Martin-Camalich, and W. Weise, Phys.Rev. **D84**, 074024 (2011), 1108.2231.
- [69] A. Semke and M. Lutz, Phys.Rev. **D85**, 034001 (2012), 1111.0238.
- [70] A. Semke and M. Lutz, Phys.Lett. **B717**, 242 (2012), 1202.3556.
- [71] X.-L. Ren, L. Geng, J. M. Camalich, J. Meng, and H. Toki (2012), 1209.3641.
- [72] M. Lutz and A. Semke, Phys.Rev. **D86**, 091502 (2012), 1209.2791.
- [73] X.-L. Ren, L. Geng, J. Meng, and H. Toki (2013), 1302.1953.
- [74] E. E. Jenkins, A. V. Manohar, J. W. Negele, and A. Walker-Loud, Phys.Rev. **D81**, 014502 (2010), 0907.0529.
- [75] A. Walker-Loud, Phys.Rev. **D86**, 074509 (2012), 1112.2658.
- [76] A. Walker-Loud, H.-W. Lin, D. Richards, R. Edwards, M. Engelhardt, et al., Phys.Rev. **D79**, 054502 (2009), 0806.4549.
- [77] C. Alexandrou et al. (ETM Collaboration), Phys.Rev. **D80**, 114503 (2009), 0910.2419.
- [78] A. C. Cordon and J. Goity, Phys.Rev. **D87**, 016019 (2013), 1210.2364.
- [79] B. Long and V. Lensky, Phys.Rev. **C83**, 045206 (2011), 1010.2738.
- [80] G. Colangelo, S. Durr, A. Juttner, L. Lellouch, H. Leutwyler, et al., Eur.Phys.J. **C71**, 1695 (2011), 1011.4408.
- [81] C. Alexandrou, E. B. Gregory, T. Korzec, G. Koutsou, J. W. Negele, et al., Phys.Rev.Lett. **107**, 141601 (2011), 1106.6000.
- [82] C. Alexandrou et al. (ETM Collaboration), Phys.Rev. **D83**, 045010 (2011), 1012.0857.
- [83] K. G. Wilson, Phys.Rev. **D10**, 2445 (1974).
- [84] B. Sheikholeslami and R. Wohlert, Nucl.Phys. **B259**, 572 (1985).
- [85] M. Luscher, S. Sint, R. Sommer, and P. Weisz, Nucl.Phys. **B478**, 365 (1996), hep-lat/9605038.
- [86] B. C. Tiburzi, Nucl.Phys. **A761**, 232 (2005), hep-lat/0501020.
- [87] G. P. Engel, C. Lang, M. Limmer, D. Mohler, and A. Schafer (BGR [Bern-Graz-Regensburg] Collaboration), Phys.Rev. **D82**, 034505 (2010), 1005.1748.
- [88] S. Capitani, M. Della Morte, G. von Hippel, B. Jager, A. Juttner, et al., Phys.Rev. **D86**, 074502 (2012), 1205.0180.
- [89] D. Toussaint (MILC Collaboration), private communication.
- [90] J. Bratt et al. (LHPC Collaboration), Phys.Rev. **D82**, 094502 (2010), 1001.3620.
- [91] R. Sommer, Nucl.Phys. **B411**, 839 (1994), hep-lat/9310022.
- [92] S. Capitani, M. Della Morte, G. von Hippel, B. Knippschild, and H. Wittig, PoS **LATTICE2011**, 145 (2011), 1110.6365.
- [93] B. Leder and F. Knechtli (ALPHA Collaboration), PoS **LATTICE2011**, 315 (2011), 1112.1246.
- [94] G. D’Agostini (1995), hep-ph/9512295.
- [95] J. Alarcon, L. Geng, J. M. Camalich, and J. Oller (2012), 1209.2870.
- [96] N. Fettes, U.-G. Meissner, M. Mojzis, and S. Steininger, Annals Phys. **283**, 273 (2000), hep-ph/0001308.
- [97] V. Pascalutsa, Phys.Rev. **D58**, 096002 (1998), hep-ph/9802288.